SAE INTERNATIONAL

Ultra-Downsizing of Internal Combustion Engines

2015-01-1252

Published 04/14/2015

Victor Gheorghiu
Hamburg University of Applied Sciences

CITATION: Gheorghiu, V., "Ultra-Downsizing of Internal Combustion Engines," SAE Technical Paper 2015-01-1252, 2015, doi:10.4271/2015-01-1252.

Abstract

The downsizing of Internal Combustion Engines (**ICE**) is already recognized as a very suitable method for the concurrent enhancement of Indicated Fuel Conversion Efficiency (**IFCE**) and the lowering of CO_2 and NO_x emissions. In this report, ultra-downsizing is introduced as an even higher stage of development of ICE. Ultra-downsizing will be implemented here by means of real Atkinson cycles using asymmetrical crank mechanisms, combined with multi-stage high-pressure turbocharging and very intensive intercooling. This will allow an increase of ICE performance while keeping the thermal and mechanical strain strength of engine components within the current usual limits.

Introduction

The scarcity of oil and gas reserves and the global warming phenomenon both urge the automotive industry towards a decrease in fuel consumption and thus a reduction in CO_2 emissions. These factors will also determine the future R&D trends for ICE.

Downsizing of ICE means simultaneous decreasing the displaced volume (usually by reducing the number of cylinders) and increasing the Indicated Mean Pressure (**IMEP**) by means of turbocharging [2], [3]. This allows the preservation of power and torque performance while decreasing the engine size. As a result, a) the mechanical and thermal losses are reduced, b) the engine becomes lighter, leading to a drop in the overall weight of the vehicle, and c) the engine operates more within its optimum fuel consumption zone. The advantages offered by a) and b) hold true even for ICE used in hybrid propulsion systems, while the advantage c) is already a feature of full-hybrid vehicles.

The level of downsizing determines the strength of the thermal and mechanical strains of engine components. In order to avoid exceeding the usual limits, either the boost pressure or the geometric (or volumetric) Compression Ratio (**CR**) must be reduced accordingly. As a consequence, the whole potential of downsizing is not achieved and the IFCE and IMEP do not reach their available maximum levels.

The current ICEs have classical (symmetrical) crank mechanisms (i.e. all four strokes of equal length) and follow the Seiliger cycle (better known in the English language as a mixed cycle). A way of improving the IFCE is the decreasing of the compression stroke. Cycles with shortened *effective* compression strokes only emulate the four stroke **Atkinson** cycle [9], because they have been implemented so far with symmetrical crank mechanisms, where the intake valves are closed very late on the cycle [1], [4], [5], [8]. Thus, a part of the charge sucked into the cylinder is pushed back to the intake pipes, and the *effective* (not the geometrical) compression stroke is decreased. This implementation of the **Quasi**-Atkinson cycle shows no noticeable improvements of the IFCE (i.e. only of the thermodynamic cycle efficiency and without any altering of the other operating parameters such as ignition timing, fuel injection strategy, AFR, EGR, cooling, sealing etc., see [2], 3, 4, [5] and Appendix 3 for more details).

There are several new series-production gasoline engines showing relatively significant benefits from either early or Late Intake Valve Closed (**LIVC**). For example Honda reports that the new gasoline engine of its Civic model gains ca. 5% fuel economy with LIVC. On the one hand, many engine parameters are adapted during this switching. For this reason, a comparison of IFCE between activated and deactivated LIVC cannot be performed correctly and thus the reported fuel economy is (from the IFCE point of view) not representative (see Appendix 3). On the other hand the knock limit improvement (and therefore the efficiency improvement) by activated LIVC comes from reducing of **effective** CR by intake closing timing rather than from reducing the geometric CR.

The Ultra-Downsizing (**UD**) is defined as a total concept consisting of several objectives and the measures required for its successful implementation. The main objectives of UD are the simultaneous increasing of the IFCE and IMEP, while reducing the emissions - particularly CO_2 and NO_x - in compliance with the usual thermal and mechanical strain limits of the engine components.

The required measures for UD implementation are processual, structural (constructive) and operational.

The processual measures include:

- The implementation of the **Real**-Atkinson cycle.
- The attempt to reach the maximum recovery of the exhaust gas enthalpy by using an optimized partition between the internal (inside the cylinder) and external (inside the turbocharger) compression (of the fresh charge) and expansion (of the exhaust gas).
- The optimization of the heat release, and of the gas exchange processes (i.e. valve timing), of the turbocharging etc.

The structural measures include:

- The use of an asymmetric crank mechanism with a (much) shorter compression stroke compared to the expansion stroke.
- The variability of the compression and expansion ratios.
- The use of (unbounded) very high-pressure turbocharging with very intensive cooling of the fresh charge before it is sucked into the cylinder etc.

The operational measures include:

- Maintaining the stoichiometric mixture in SI engines and decreasing of the Air-Fuel-Ratio (**AFR**) while observing soot limits in CI engines at every Engine Operating Points (**EOP**), which would enable the use of either a 3-way catalytic converter for NO_x reduction or a less frequent regeneration of the NO_x storage catalytic converter.
- The continuous adjustment of the compression ratio to the available boost pressure for performing the load control mostly without throttling, leaning and stratifying of the mixture and/or intensive external EGR.
- The thermodynamic shutdown of the cylinder by shutting off the fuel supply and by significantly reducing the compression ratio.

Old and New Implementations of the Quasi-Atkinson Cycle on ICE with Classical (Symmetrical) Crank Mechanism

Naturally Aspirated Engines

The market share of hybrid vehicles, most of them using Spark Ignition (**SI**) engines, has been steadily increasing over the past years. For example Toyota uses in its Prius II [1] and III [8] a SI engine which tries to achieve a higher IFCE by using a Quasi-Atkinson cycle, where the intake valve is kept open for a large part of the compression stroke and the geometric compression ratio is enhanced. Consequently, in the initial stage of the compression stroke (when the piston begins to ascend), some of the air that had entered the cylinder is returned to the intake manifold, in effect delaying the start of compression. In this way, the expansion ratio is increased without increasing the *effective* compression ratio. Sophisticated variable valve timing is used to carefully adjust the intake valve timing to operating conditions in order to reach maximum efficiency.

Many variants of this implementation of the Quasi-Atkinson cycle were evaluated in detail in [5]. It has been proved by simulations in [5], that the pushing out of residual gases during the exhaust stroke consumes more piston work in the Quasi-Atkinson cycle (compared to the Seiliger cycle) because of the lower pressure at the exhaust valve opening (as a result of the extended expansion) and consequently of the sluggish cylinder emptying process. The oscillating air stream from and to the intake manifold through the intake valve port (because of the flow losses) reduces considerably the IFCE of the Quasi-Atkinson cycle. The increased CR shows a very positive effect on the IFCE during the expansion stroke so that, finally, the IFCE of the Quasi-Atkinson cycle comes close to or even exceeds slightly the level of a classical Seiliger cycle. One can conclude that the IFCE gain of this kind of Atkinson cycle implementation is modest and largely dependent on the fine tuning of all parameters (valve timing etc.). In addition, the specific power of the engine is low because of the lower retained mass of fresh change in the cylinder before compression. This means that either LIVC is activated only for part loads or a relatively large and therefore heavy engine (due to the large displacement) is needed to power the vehicle. The most IFCE improvement in the case of Prius II and III for example is obtained by means of shifting the EOP in areas with maximal IFCE and controlled electrical driving of accessories (i.e. electric water pump). For these reasons, this implementation of the Quasi-Atkinson cycle is suitable only for hybrid vehicles, where the engine - because it is not linked mechanically directly to the wheels, nor controlled by the driver - works only in its best operating range.

Turbocharged Engines

First, we analyze the commonly used practice of concomitant suction delaying and the increase in boost pressure. In order to achieve the same maximum values of pressure and temperature on all cycles at virtually the same IMEP, the AFR must be adapted. The placement of the combustion phase on all cycles is kept unchanged. The number of parameters influencing the turbocharged engines becomes much higher compared to the aspirated engines. As a consequence, the effort to achieve the combinations of parameters which maximize the IFCE of such engine cycles becomes much bigger.

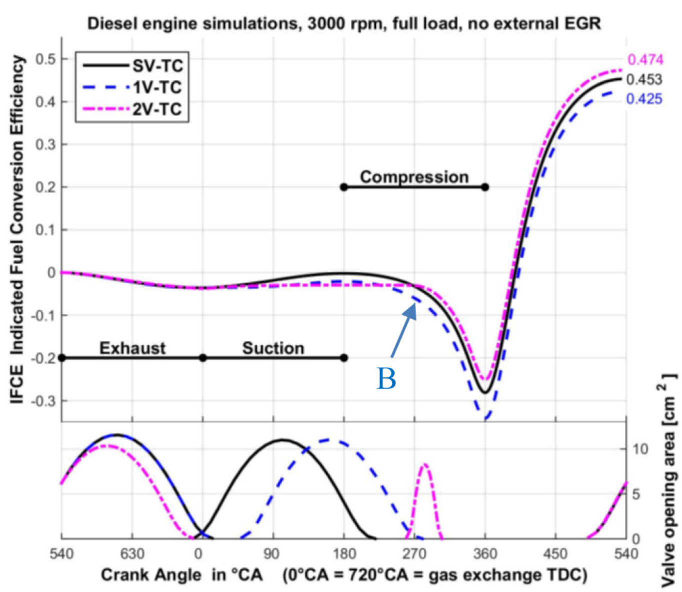

Fig. 1. Indicated Fuel Conversion Efficiency, Crank Angle - Diagram

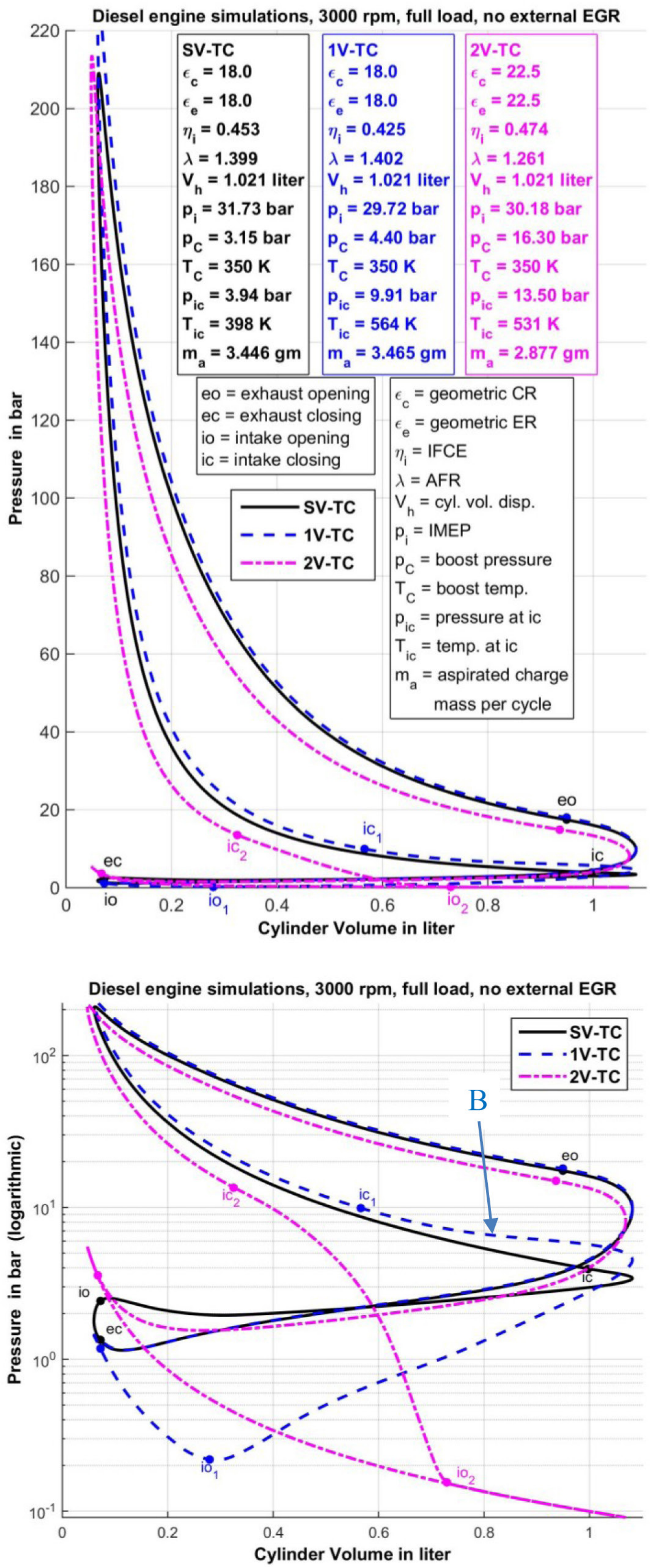

Fig. 2. Pressure, Volume (top) and Pressure (logarithmic), Volume - Diagrams with the valve timing states.

The simulation results for the 1st variant of Quasi-Atkinson cycle implementation (labelled here as **1V-TC**), where the intake valve closing is 60°CA delayed, are presented in Figures 1, 2, 3. Due to the delayed suction, the gas exchange processes are very different from the standard version of the Seiliger cycle (labelled here as **SV-TC**). During the exhaust stroke, there are no major differences in IFCE between the cycles (see Fig. 1). The boost pressure (pC) is increased to achieve nearly the same filling rate of the cylinder (m_a) (see Fig. 3) and thus the same IMEP, (see the values in the table from Fig. 2). The oscillating air stream from and to the intake manifold through the intake valve port (see B area in Fig. 3), reduces considerably the IFCE (see B areas in Fig. 1 and 2 and its final value in the table from Fig. 2) of the cycle.

In the 2nd variant of the Quasi-Atkinson cycle implementation (a new one, labelled here as **2V-TC**), the suction process is much more delayed and a very high boost pressure (pC of more than 16 bars at the unchanged boost temperature TC) is taken into consideration. Due to the delayed suction less mass is aspirated into cylinder (see Fig. 3).

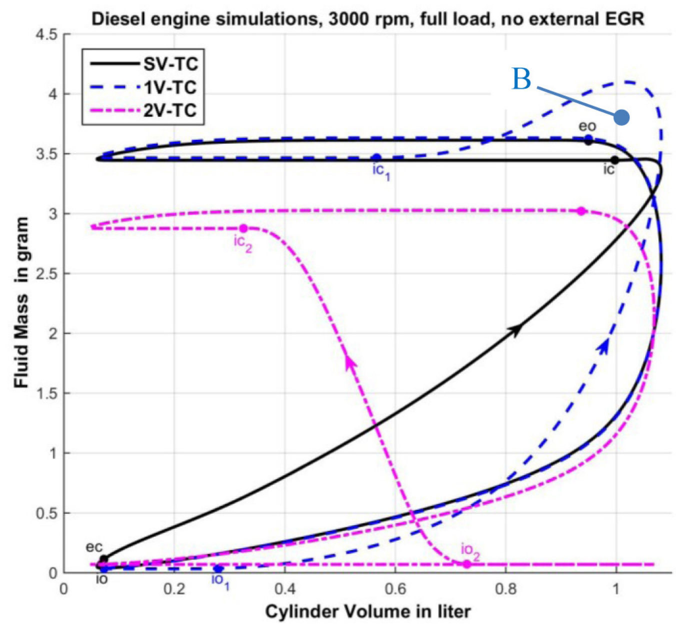

Fig. 3. Fluid Mass, Volume - Diagram with the valve timing states.

For improving the indicated IFCE of this cycle, the CR is increased by 22% compared to the Seiliger cycle (SV-TC). Special characteristics of the 2V-TC Quasi-Atkinson cycle implementation are: a) the residual gases are expanded during the suction stroke and then compressed, as in the Miller cycle [4] and b) the suction of fresh charge starts first, after the full completion of the suction in Seiliger cycle, and takes a very short time. The major impact of the decrease in compression work in this variant can be seen clearly after the closing of the intake valve (see Fig. 1). In short, although the boost pressure in the 2V-TC Quasi-Atkinson cycle implementation is more than five times higher at virtually the same IMEP, only a minor improvement of the IFCE can be detected.

For this reason, the implementation of such Quasi-Atkinson cycles does not represent a suitable solution. Therefore, a new approach is needed to implement real Atkinson cycles.

Implementation of Real-Atkinson Cycles on ICE with Asymmetrical Crank Mechanisms (ACM)

In order to realize a strict Atkinson cycle - i.e. geometrically shortened compression and extended expansion strokes - special crankshaft drives are needed. The main aim here is merely to estimate the potential for increasing the IFCE if an asymmetrical crankshaft drive is used. In other words, this strict implementation of the Atkinson cycle, labeled further on as Real-Atkinson, investigates the extent to which losses caused by the suction and partial expulsion of the fresh charge reduce the IFCE.

Similar investigations for naturally aspirated engines have already been published in [5] and are therefore not presented and analyzed in this paper.

Turbocharged Engines

The limitation of the maximum pressure during the cycle determines the CR - boost pressure pair of parameters. If a relatively high boost pressure is desired, the CR must be reduced accordingly in order to accomplish the maximum pressure limitation of the cycle. This will also decrease the IFCE since it is determined primarily by the CR. Furthermore, the expansion inside the cylinder occurs largely incompletely and the exhaust gases exit the cylinder with a still too high specific enthalpy, which decreases the IFCE even further. However, the expansion of exhaust gases in the turbines, with its high specific enthalpy, can be used only in part to drive the compressors and, therefore, to enhance the boost pressure because it exceeds the upper pressure limit of the cycle.

The following facts can be used to summarize the current situation:

- To raise the IFCE, most of the working gas expansion should occur within the cylinder and most of its compression outside the cylinder, i.e. within the compressor.
- If the expansion process occurs entirely within the cylinder (ideally, a full expansion occurs up to the ambient pressure), no additional boost pressure by means of the TC can be generated. Moreover, a long expansion stroke (and, therefore, an engine with a long piston displacement) is necessary. However, that leads to a high IFCE but quite low indicated specific power (kW/L) and IMEP of the engine.
- In order to simultaneously increase the IFCE and the IMEP, the engine must have variable CR, must be highly turbocharged and the ratios between the internal and external expansions and compressions together with the CR must be simultaneously optimized.
- To be able to accomplish these optimizations, an asymmetrical crank mechanism (ACM) is required.

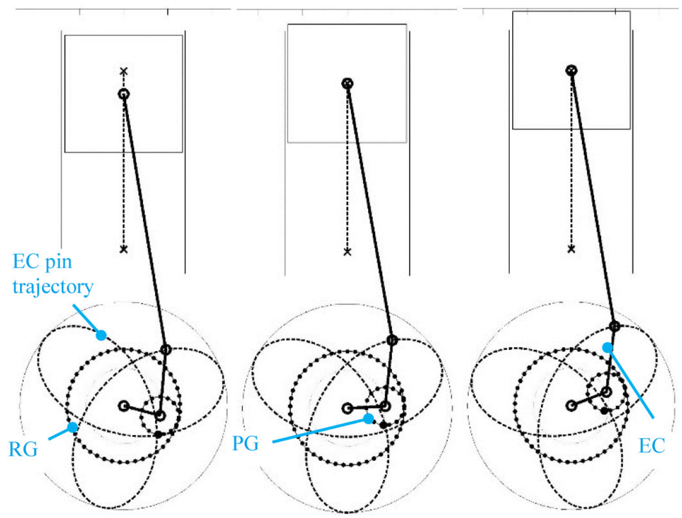

Fig. 4. Schematic Representation of the 2nd Variant of the ACM - consisting of held Ring Gear (RG), Planet Gear (PG) with Eccentric Crank (EC) - in the combustion TDC position for three CR. The adjustment of the CR are obtained by ± twisting of the RG with respect to the middle position (see Appendix 2 for more details).

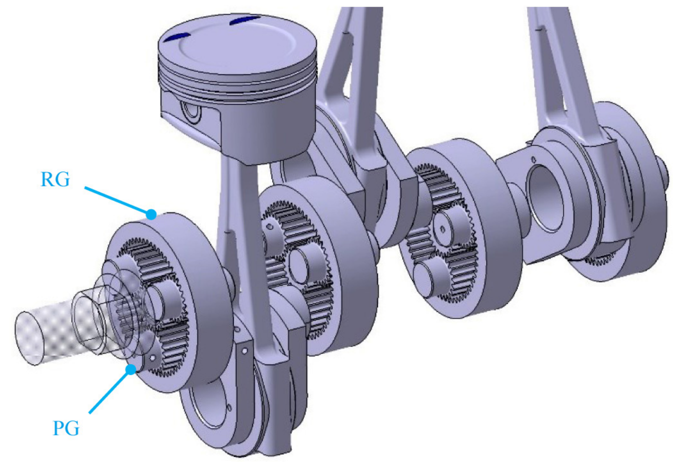

Fig. 5. CAD Model of the 2nd Variant of ACM for a 3 Cylinder Engine

The ACM used here (see Fig. 4 for schematic and Fig. 5 for CAD representations, and Appendix 2) can be dimensioned accordingly to realize the piston displacements for the Real-Atkinson cycles with a given asymmetry between the compression and expansion strokes (see Fig. 6A) and enable for each chosen asymmetry the variation of the CR (see Fig. 4 and 6B). This 2nd variant of the ACM from [10], [11] has the 3:1 ratio between the teeth number of the ring and planet gears. Therewith the four strokes are generated in only one revolution of the crankshaft, just as in the original Atkinson patent [9].

The working principle of such ACM has been known since 1919 [12] and therefore will not be described in detail (see Appendix 2 for more details).

The simulations are carried out in the following **two investigation cases** with the purpose of looking for the optimum ratio between the internal and external expansions, which leads simultaneously to maximizing the IFCE and enabling sufficiently high values of IMEP:

1. In the Investigation Case A (**IC A**), the simulated variants are based on a steady geometric Expansion Ratio (**ER**) and a varied CR. This means that the identical expansion and exhaust strokes are kept unchanged while the identical intake and compression strokes are varied significantly - by means of varying the eccentric radiuses "exx" (see legend of Fig. 6A, Fig. 4 and Appendix 2) of the ACM - in order to allow the modification of the ratio between internal and external expansion.
2. In the Investigation Case B (**IC B**), the simulated variants are based on a steady eccentric radius (e32) where ER, CR, the geometric Intake Ratio (**IR**) and the geometric Exhaust Ratio (**XR**) are varied simultaneously by means of the parameter "g", i.e. of the twisted angle of the ring gear (see Fig. 4 and the legend of Fig. 6B).

The simulation tool used in this paper for turbocharged engines is the BOOST® from AVL Co (see as example the model from Fig. 7).

The power balance of turbochargers determines the actual boost pressure level of the engine. The turbochargers (**TC**) are modeled for these investigations in a simple manner. It describes the expansion process in the turbines (**Tx**) by means of their discharge coefficients while the air compression within the compressors occurs up to a maximum pressure ratio which depends on the available turbine output.

To be able to simulate cycles with very high boost pressures as well, three intercooled TCs are placed in line (three-stage turbocharging, see Fig. 7). When the boost pressure required for preserving the pressure limit on the cycle is low, the superfluous TCs are kept in use for simplicity and comparability (i.e. are not bypassed). In this case the expansion and compression ratios of the turbines and compressors tend gradually toward 1, i.e. these TCs switch off themselves thermodynamically (see Fig. 10A, 11A, 12A).

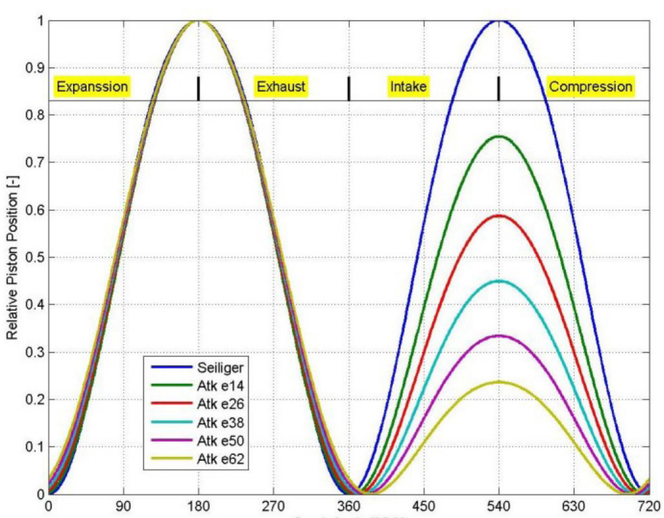

Fig. 6A. Relative Piston Position, Crank Angle - Diagram for the 1st variant of the ACM (see Appendix 2) used in the IC A. The abbreviations "exx" denote the length of the eccentric crank (EC).

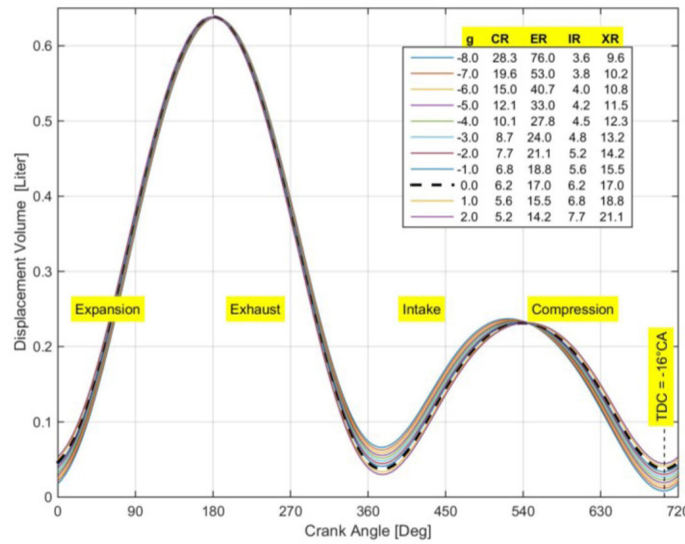

Fig. 6B. Displacement Volume, Crank Angle - Diagram for the 1st variant of the ACM (see Appendix 2) used in the IC B. The parameter "g" denote the twisting angle of the ring gear (RG) with respect to the middle position (g = 0). The table shows the dependency of the geometric compression (CR), expansion (ER), intake (IR) and exhaust (ER) ratios of the parameter "g".

Most parameters of the BOOST model are selected for a hypothetical engine and are kept unchanged for all these simulations. This includes parameters such as all geometrical dimensions (with the exception of the crank mechanism), valve timing, wall temperatures (300 K) and heat transfer coefficients (Re-analogy) of the pipes, as well as the efficiencies and pressure losses of the intercoolers (target efficiency = 0.75, target pressure drop = 5 kPa) and friction coefficients in the pipes (0.019). Likewise, the efficiency of the turbochargers (compressor efficiency = 0.75, turbocharger overall efficiency = 0.5), as well as the blow by gap size of the cylinder, frictional characteristic curve of the engine and AFR - the combustion parameter (see Table 1A) - are also included. A simple Vibe function for the heat release is selected in order to model the combustion process. The different positions of the TDC in the Atkinson and Seiliger cycles (see Fig. 6A) are compensated by choosing a suitable start of combustion (**SOC**), so that combustion begins uniformly in all cycles at 15°CA before TDC.

The Table 1A shows the ER (geometric expansion ratio), CR (geometric compression ratio), μ_{Tx} (turbine discharge coefficients), n (engine speed), AFR (air-fuel ratio), SOC (start of combustion), CD (combustion duration), m_{Vibe} (exponent of Vibe function for the cylinder heat release modeling), IFCE (indicated fuel conversion efficiency), IMEP (indicated mean pressure), max(p) and max(T) (maximum pressure and temperature during the cycle), p_{MP8} and T_{MP8} (mean boost pressure and temperature; i.e. at the measuring point MP8, see Fig. 7) and p_{MP12} and T_{MP12} (mean exhaust back pressure and temperature; i.e. at MP12, see Fig. 7) for cylinder 1.

Table 1A. Parameter (top) and Performance (bottom) for IC A (comma means decimal point!)

Cycle	ER	CR	μ_{T1}	μ_{T2}	μ_{T3}	n	AFR	SOC	CD	m_{Vibe}
	-	-	-	-	-	rpm	kg/kg	°CA	°CA	-
Atk e14	27,0	20,6	0,480	0,258	0,161	3000	14,6	-21	86	1,5
Atk e26	27,0	16,2	0,430	0,231	0,144	3000	14,6	-24	86	1,5
Atk e38	27,0	12,7	0,335	0,180	0,112	3000	14,6	-30	86	1,5
Atk e50	27,0	9,7	0,256	0,138	0,086	3000	14,6	-36	86	1,5
Atk e62	27,0	7,1	0,199	0,106	0,067	3000	14,6	-42	86	1,5
Seiliger	7,0	7,0	0,330	0,177	0,111	3000	14,6	-15	86	1,5
Seiliger	15,0	15,0	0,620	0,333	0,208	3000	14,6	-15	86	1,5

Cycle	ER	CR	IFCE	IMEP	max(p)	max(T)	p_{MP8}	T_{MP8}	p_{MP12}	T_{MP12}
	-	-	-	bar	bar	K	bar	K	bar	K
Atk e14	27,0	20,6	0,419	25,7	231	2209	3,02	336	2,79	867
Atk e26	27,0	16,2	0,423	28,2	234	2197	4,08	343	3,78	877
Atk e38	27,0	12,7	0,423	27,9	237	2182	5,13	346	4,79	877
Atk e50	27,0	9,7	0,413	26,7	235	2167	6,55	348	6,16	913
Atk e62	27,0	7,1	0,391	24,6	229	2152	8,78	356	8,07	915
Seiliger	7,0	7,0	0,301	57,9	232	2292	12,48	450	15,85	1396
Seiliger	15,0	15,0	0,383	42,1	232	2344	4,62	361	4,62	1127

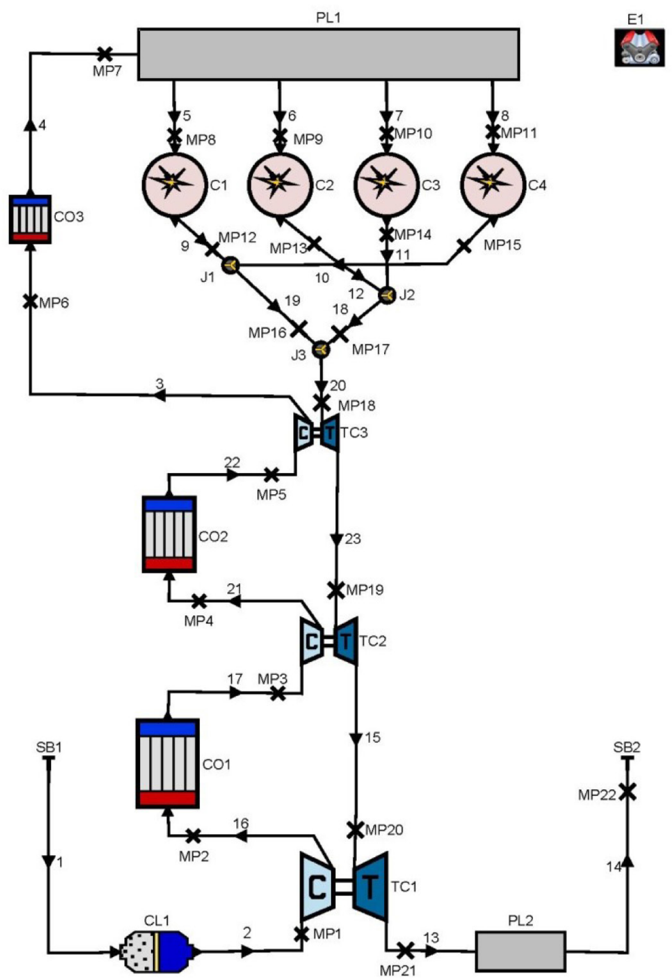

Fig. 7. BOOST model of a four cylinder turbocharged engine. Simple numbers denotes pipes, Cx = cylinder, COx = cooler, TCx = turbochargers, PLx = plenum, Jx = junctions, CLx = cleaner, SBx = system bounda-ries, Ex = engine and MPx = measuring points

The various parameters from Table 1A for the **IC A** and from Fig. 15B for the **IC B** are selected for the purpose of obtaining roughly the same maximum cylinder pressure max(p) ≈ 230 bar in all cycles. In order to reach this state, the discharge coefficients of the three turbines (μ_{T1}, μ_{T2} and μ_{T3}) are varied according to a) the influence of the back pressure behind the cylinder (e.g. at the measuring point MP12 for cylinder 1; see Fig. 7) and of b) the boost pressure (e.g. at MP8 for cylinder 1). In order to reach approximately the same expansion rate in all three turbines, their discharge coefficients are set at the same level and compensated with the cross sections ratios of the turbine output pipes. Hence, only the discharge coefficient of the third turbine μ_{T3} is adapted for each cycle to meet the cylinder peak pressure limit, since this sets the level of the other two discharge coefficients μ_{T2} and μ_{T1} (see Table 1A and Fig. 15B).

Simulation Results and Trends for the IC A

All Atkinson cycles show better IFCE values than the Seiliger cycles (see Fig. 8A). However, the Seiliger cycles reach higher IMEP values because of the longer intake stroke and, therefore, the larger gas mass sucked in (see Fig. 13A). Furthermore, higher boost pressures p_{MP8} are required in both the Atkinson and Seiliger cycles in order to hold the parameter max(p) steady when the CR is reduced (see Table 1A).

The comparison of the Atk e62 (with CR = 7.1) and Seiliger (with CR = 7) cycles shows that a) the Atkinson cycle has a 30% higher IFCE and reaches 58% less IMEP and b) the Seiliger cycle needs a 30% higher boost pressure (p_{MP8} in Table 1A) and must overcome a 50% higher cylinder back pressure - i.e. before T3 (p_{MP12} in Table 1A). Moreover, the comparison of the Atk e38 & e26 (with CR = 12.7 respective = 16.2) and Seiliger (with CR = 15) cycles shows that the Atkinson cycles have a 10% higher IFCE (although the maximum cylinder temperature max(T) is ca. 160 K, i.e. 7% lower) and a 34% lower IMEP. The highest IFCE value for the Atkinson cycles is not reached in the variant with the highest CR, but in the variant with a CR of about 50% of the ER. Consequently, the optimum variant features an intake stroke equal to approx. 50% of the expansion stroke.

Some diagrams are introduced and analyzed below in order to determine the cause of these trends. The pressure-volume diagram of all cycles is presented in Fig. 9A and the pressure-specific volume diagram of the intake and the exhaust gas paths of each Seiliger and Atkinson cycle are presented in Fig. 10A. It can be inferred from Table 1A, as well as recognized in Fig. 9A and 10A, that the Seiliger cycle where the CR = 7 needs the highest boost pressure to reach the desired max(p) ≈ 230 bar (because of its low CR). The consequences are an extremely high back pressure p_{MP12} (see Fig. 9A and 10A) and falling ISFC because of the very intensive exhaust work required to push the exhaust gases out of the cylinder (see in Fig 9A the curve up to exhaust valve closing "ec" point). Therefore, this cycle occurs exclusively in the pressure range above 10 bar. For the Atkinson cycle Atk e38, this situation is reversed (see Table 1A and Fig. 9A for comparison). This cycle occurs exclusively in the pressure range above 5 bar.

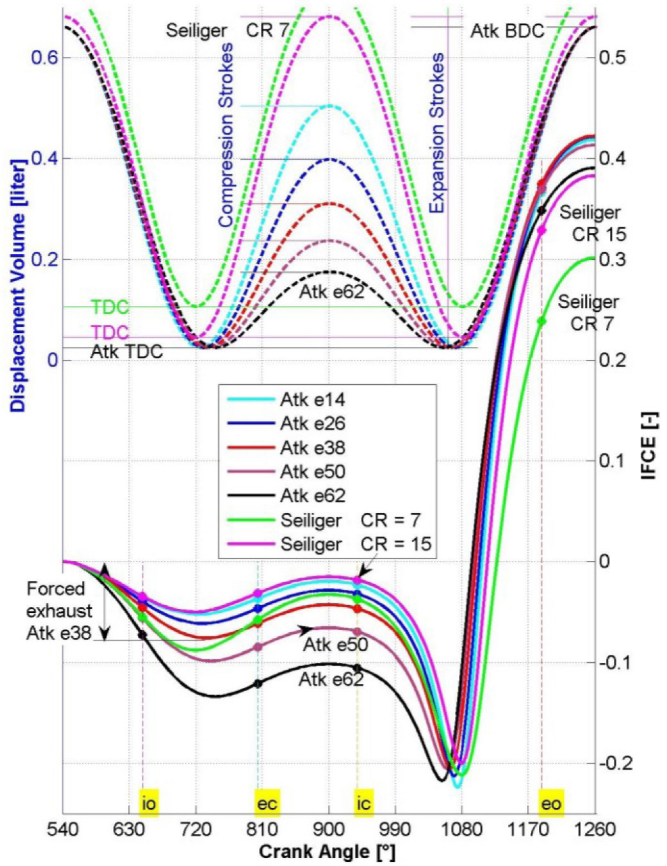

Fig. 8A. Displacement Volume, CA - Diagram (top curves with left axis) and IEFC, CA - Diagram (bottom curves with right axis) with valves timing states

The differences between both cycles can be clearly seen in the intake and exhaust gas paths. Fig. 10A and 11A show the three-stage compression of the air and all the states after passing through each compressor and intercooler (with the associated pressure losses). Fig. 10A and 12A show the three-stage expansion of the exhaust gases in the turbines. Fig. 12A shows, that the discharge coefficients are properly adapted between the turbines because the expansion occurs almost linearly in all three stages.

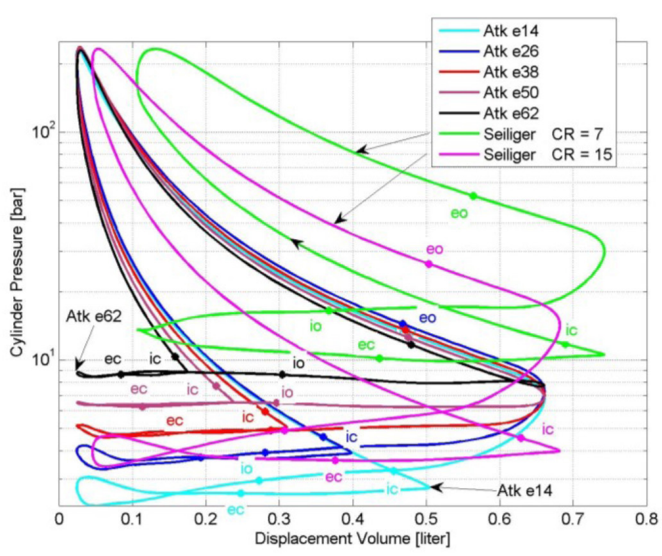

Fig. 9A. Pressure (logarithmic), Volume - Diagram with valves timing states (see Abbreviations)

The air compression and the exhaust gas expansion for the cycle Atk e38 occur mostly in TC3 (see Fig. 10A) because the exhaust gas pressure at the MP18 point (i.e. before T3) is too low (see also Table 1A) to be able to adequately drive T2 and T1. Consequently, the exhaust gases compress partly in T2 and T1 instead of expanding (see MP19 to MP21 in Fig. 10A). No modification of the IFCE sequence between variants is obtained by deleting TC1 from the BOOST model (i.e. there is no need to remove the unnecessary TC in these simulations).

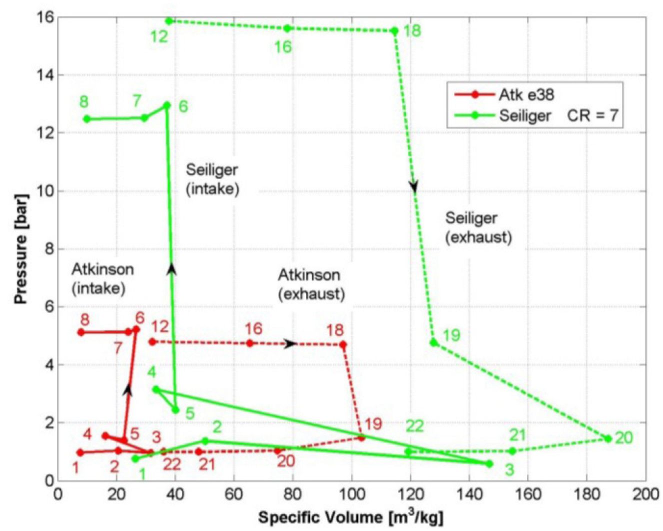

Fig. 10A. Pressure, Specific Volume - Diagram. The numbers shown here and in the next diagrams denote the Measuring Points states (see MPx in Fig. 7).

In all Atkinson cycles, the sucked intake gas mass changes minimally (see the red circle area on the left side of Fig. 13A), i.e. IMEP follows preponderantly the IFCE variation and is, for the most part, independent of the boost pressure (p_{MP8}) variation.

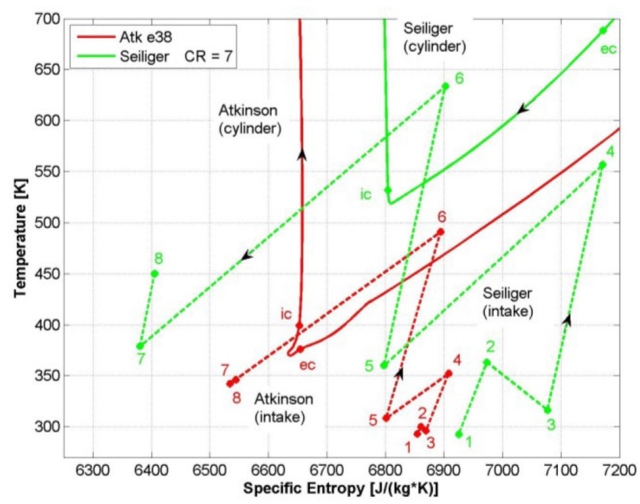

Fig. 11A. Temperature, Specific Entropy - Diagram in Cylinder & Intake Path. The Abbreviations "ec" and "ic" denote the valve timing states.

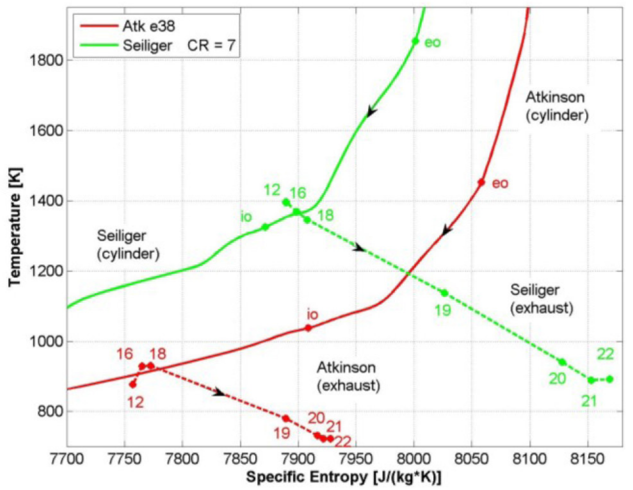

Fig. 12A. Temperature, Specific Entropy - Diagram in Cylinder & Exhaust Path. The Abbreviations “eo” and “io” denote the valve timing states.

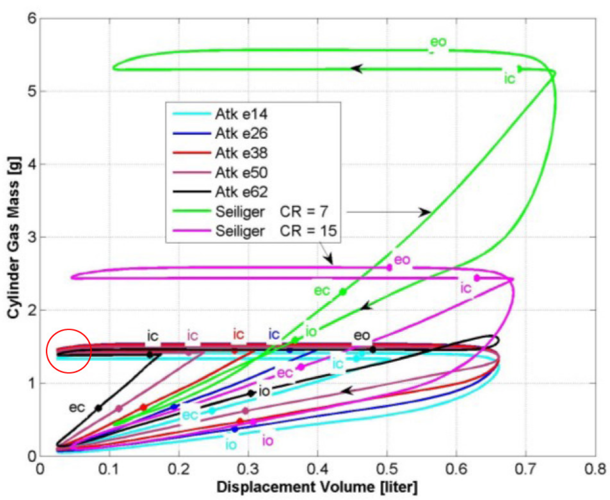

Fig. 13A. Fluid Mass, Volume - Diagram of Atkinson and Seiliger Cycles.

Simulation Results and Trends for the IC B

A number of trends become clear after analyzing the parameters and performances presented in Fig. 15B and 17B.

This type of crank mechanism - which permits the CR variation (in this case via parameter “g”) - enables the implementation of Real-Atkinson cycles for part and full-load EOPs, where the IMEP varies between 8.5 and 42 bar, even with the stoichiometric AFR and without throttling. Moreover, the IFCE in all these EOPs only varies within a 6% band (related to its maximum value, see also Fig. 14B and 17B). In all these EOPs, the maximum cylinder pressure remains at approx. 230 bar and the maximum cylinder temperature varies between 1800 and 2300 K (see Fig. 17B). The optimization of the heat release could significantly reduce the maximum cylinder temperature. In variant “g+2” (see legend), the maximum boost pressure (p_{PM8}) reaches nearly 12 bar, while the boost temperature (T_{PM8}) does not exceed 360 K (see Fig. 17B).

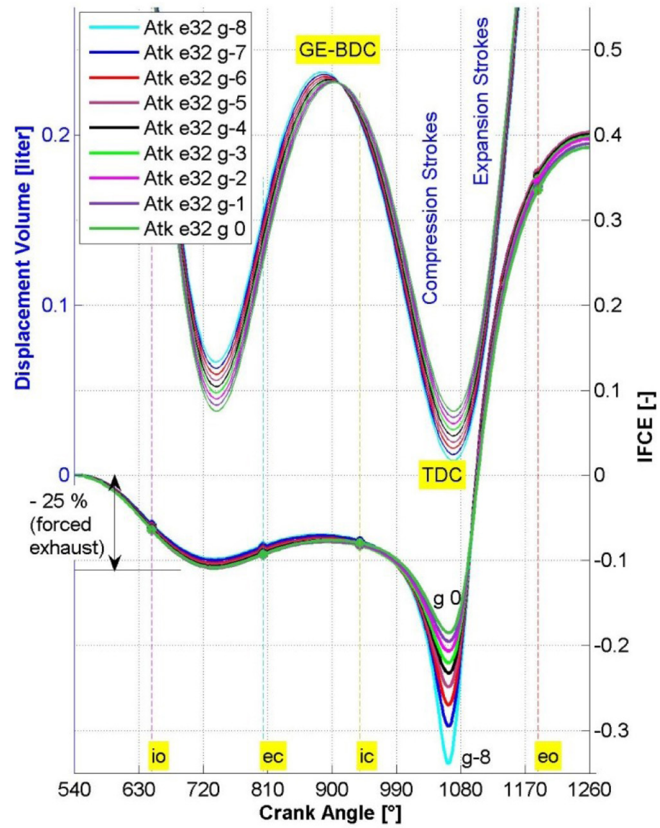

Fig. 14B. Displacement Volume, Crank Angle - Diagram (top curves, left axis) and IEFC, Crank Angle - Diagram (bottom curves, right axis)

In this case, the cylinder is filled to maximum (see Fig. 18B). As a result of the extended expansion within the cylinder (see Fig. 16B) the exhaust gas temperatures before turbine T3 (T_{MP12}) only reach a maximum of 1000 K (see Fig. 17B). This means that the turbine wheel does not need to be protected against a higher gas temperature, but, at the same time, a higher exhaust gas pressure is required before T3 (p_{MP12}) in order to achieve the desired boost pressure (p_{MP8}).

The required higher exhaust gas pressure before T3 (p_{MP12}) (i.e. the cylinder back pressure) significantly diminishes the IFCE (i.e. by approx. 25%, see IFCE variation in Fig. 14B between 540°CA and the “ec” position). The load independence of these IFCE losses is quite unexpected, but if the difference between the cylinder pressure at “eo” and the back pressure (p_{MP12}) in Fig. 16B is noted, the positive effect of the exhaust gases released from the cylinder (i.e. of the free exhaust) becomes evident. An additional optimization of the valve timing can considerably reduce the back pressure and, therefore, these IFCE losses.

The residual gas concentration decreases, while the XR and boost pressure increase (see Fig. 17B). The increase in the XR makes the cylinder exhaust more complete and the increase in boost pressure favors the scavenging of residual gases from the cylinder.

The IMEP enhancement - from 8.5 to 42 bar, while AFR remains unchanged (here stoichiometric) and IFCE only varies within a 6% band - is the result of more gas mass aspirated into the cylinder (see Fig. 18B).

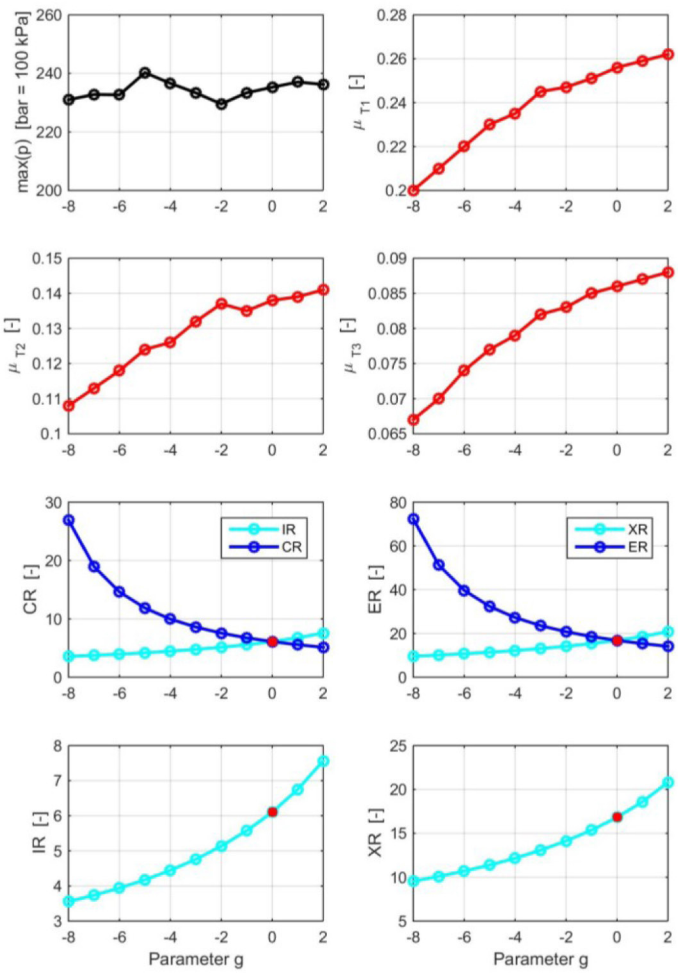

Fig. 15B. Parameters for the IC B over Parameter "g" (i.e. over the twisting angle of the ring gear) respectively over CR variation (see table from Fig. 6B for the parameter "g" and CR correlation).

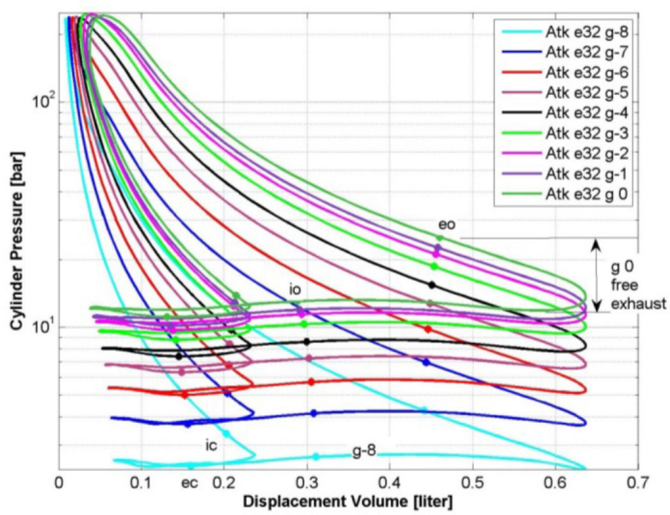

Fig. 16B. Pressure (logarithmic), Volume - Diagram for Atkinson-Cycles for many values of the Parameter "g" respectively of the CR (see table from Fig. 6B for their correlation). The "free exhaust" denotes the drop in pressure between exhaust opening "eo" and the backpressure of the cylinder.

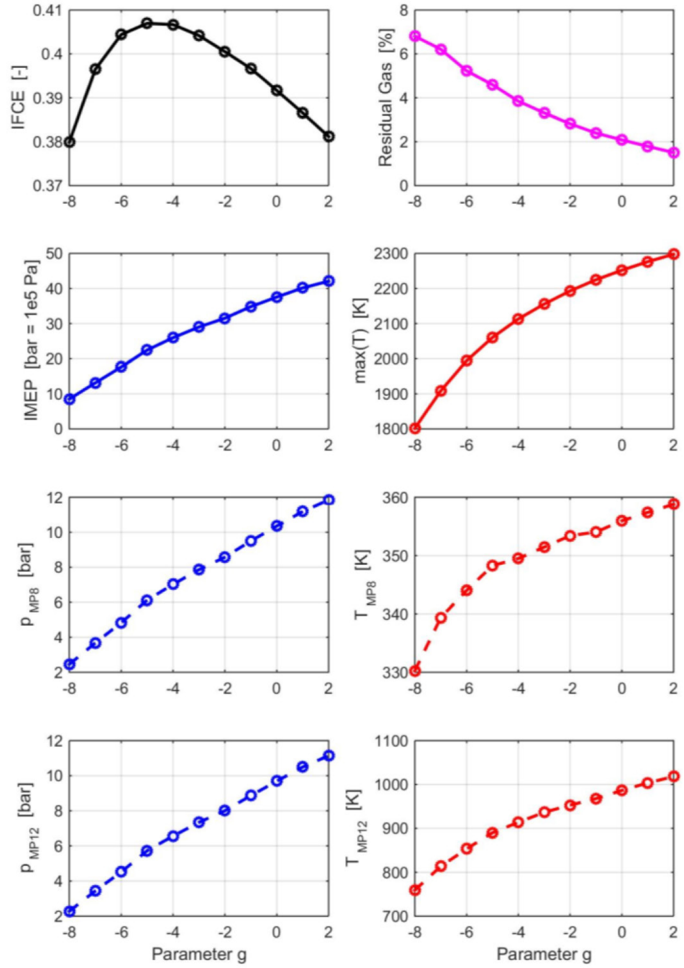

Fig. 17B. Performance for the IC B over Parameter "g"

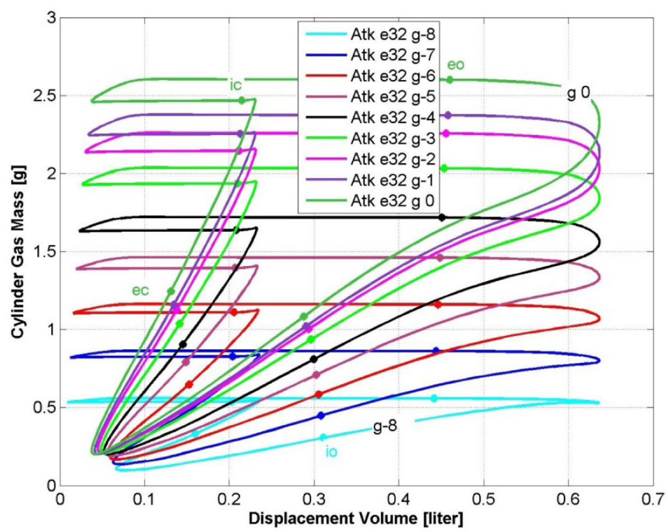

Fig. 18B. Fluid Mass, Volume - Diagram

Evaluation of the Highest IFCE Values of the Seiliger and Atkinson Cycles

The Ideal V,p,T - Model for the Open Seiliger and Atkinson Cycles

Because in the case of the supercharged ICE, the number of parameters which influence the IFCE and BMEP is very high, the attempt to find combinations of parameters which maximize the performances of the real (by BOOST) ICE cycle becomes very difficult. For these reasons, ideal models of the V,p,T-Seiliger and -Real-Atkinson cycles have been developed (see an old version in [5] and the new one in the Appendix 1).

Modeling by means of V,p,T-cycles has the advantage of allowing users to generate ideal ICE cycles which model more closely the real cycles than the classic ideal V- and V,p-cycles by observing their mechanical (pressure) and thermal limits. A simple V-cycle (Otto cycle), where the heat is released only in an isochoric manner (i.e. by constant volume), generates unrealistically high levels of maximum pressure and temperature during the cycle. The attempt to limit the maximum pressure level leads to the classic V,p-cycle [6], [7], where the heat is released in an isochoric and isobaric (constant pressure) manner. The V,p-cycles (i.e. classic Seiliger cycles) leads, for example, to very high temperature levels in the case of fully loaded supercharged engines. These levels are completely unrealistic.

In the ideal V,p,T-cycle, the heat is partially released isochorically on the 2 - 3v change of states, isobarically on 3v - 3p and isothermally on 3p - 3 (see states noted in Fig. 19). The amounts of heat released isochorically and isobarically depend on the targets for maximum pressure and temperature of the cycle. The theoretical background of this ideal open cycle (i.e. with gas exchange) is presented in detail in the Appendix 1.

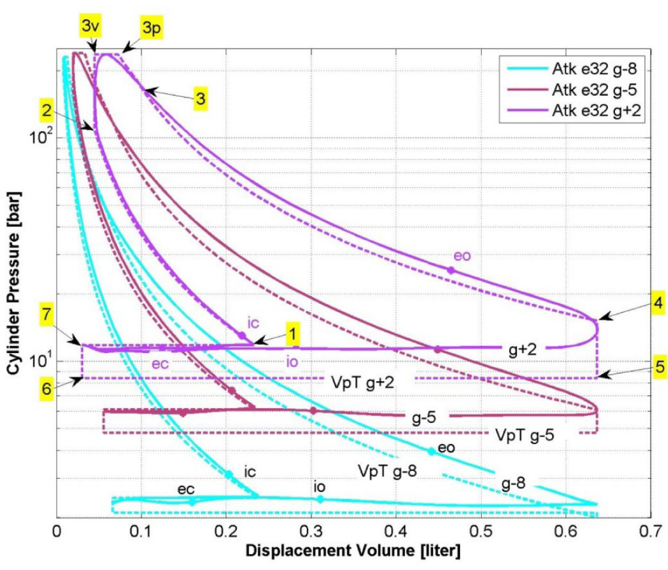

Fig. 19. Pressure (logarithmic), Volume - Diagram for Boost (with Valves Timing) and V,p,T (dashed curves) for three Values of Parameter "g" i.e. of CR

In the ideal V,p,T-model, the thermal properties of the working fluid (κ_c for the unburned and κ_e for the burned parts) are kept constant throughout the cycle. The entire fuel mass is added to the cylinder gas mass in the "3v" state of the cycle (see Fig. 19). The mass contribution of the exhaust residual gas part is also taken into consideration. The available heat (from fuel combustion) decreases by the amount of heat transferred to cylinder wall. In this case, the compression, combustion and expansion can be treated adiabatically. The backpressure behind the cylinder p_T (equivalent of the p_{MP12} from the BOOST model) is computed by means of energy balance at the turbocharger.

In order to be able to compare the simulation results, the following parameters are carried over from the BOOST to the V,p,T-model: p_C, T_C, p_{max}, T_{max}, m_1, m_f, κ_c, κ_e, Q_{wall} (see Appendix 1 for their meaning).

The diagrams of cylinder pressure over displacement volume from Fig. 19 show a relatively good concordance for the high pressure part of the cycles. The heat release and heat transfer to cylinder wall are responsible for most of the differences. The V,p,T-model features an optimal heat release, i.e. the maximum achievable isochorically and isobarically parts for reaching the target values for maximum pressure and temperature of the cycle. The gas exchange and turbocharging processes used in the V,p,T-model are also optimal. The parameter and performances of the BOOST and V,p,T-cycle simulations are shown in Fig. 20 and 21.

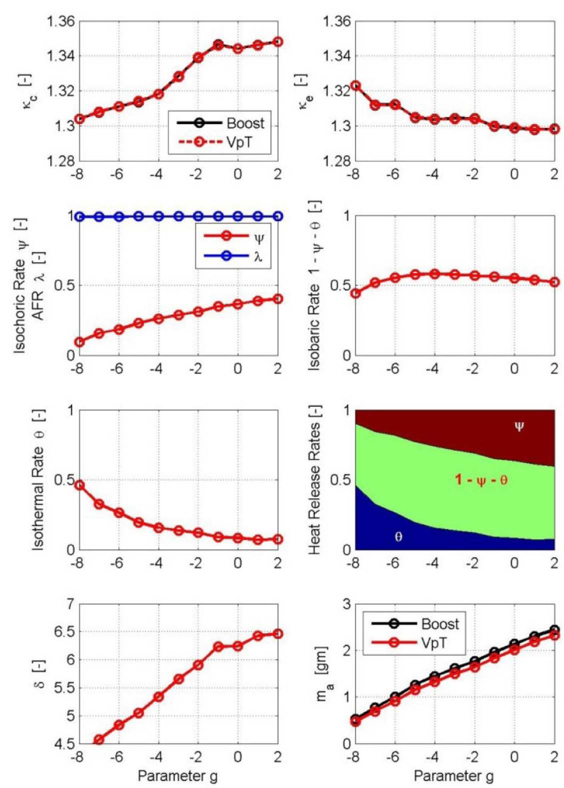

Fig. 20. Parameter for V,p,T-model over Parameter "g"

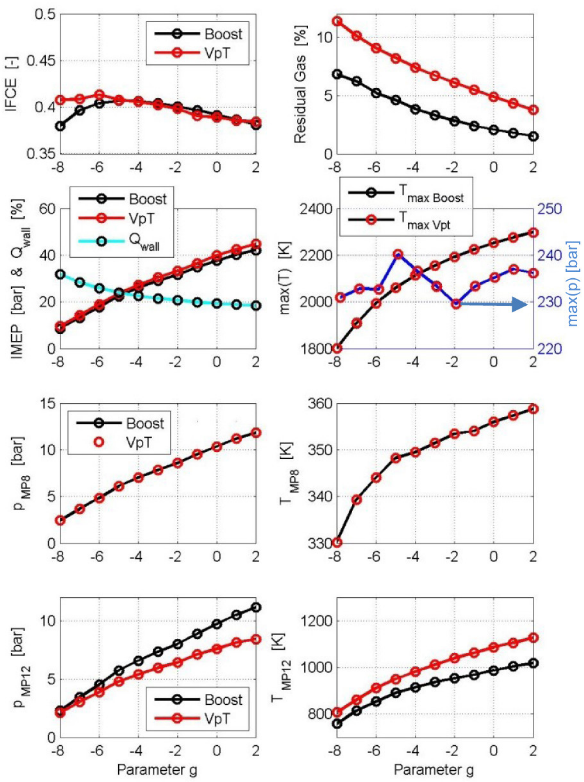

Fig. 21. Performance for V,p,T-model over Parameter "g". The correlation between CR and Parameter "g" is presented in Fig. 15B.

Comparison between the Performances of the Seiliger and Atkinson Cycles by Means of the V,p,T-Model

The V,p,T-model is used to simulate both cycles while preserving the same settings for:

- CR ε_c,
- AFR λ,
- heat release rates (i.e. isochoric ψ, isobaric $1-\psi-\theta$ and isothermal θ),
- heat transfer rate to the cylinder wall ξ_{wall},
- pressure at the end of compression p_2,
- boost pressure p_C and boost temperature T_C,
- free exhaust ratio $\phi_{ex} = p_4 / p_5$,
- overall turbocharger efficiency η_{TC},
- maximal cylinder displacement etc.

In this way, the big effort of optimizing all the BOOST model parameters (such as heat release, valves timing etc.) can be avoided and an accurate comparison between the performances of the Seiliger and Real-Atkinson cycles is enabled.

The 2nd Variant of the Asymmetrical Crank Mechanism used for these investigations enables the simultaneous variation of the geometric ratios and (more reduced) of the piston strokes from Fig. 22 and Fig. 23. The maximum cylinder displacement remains nearly unchanged, when the CR are varying between 5.1 and 18.1 (see Fig. 22 and Fig. 23).

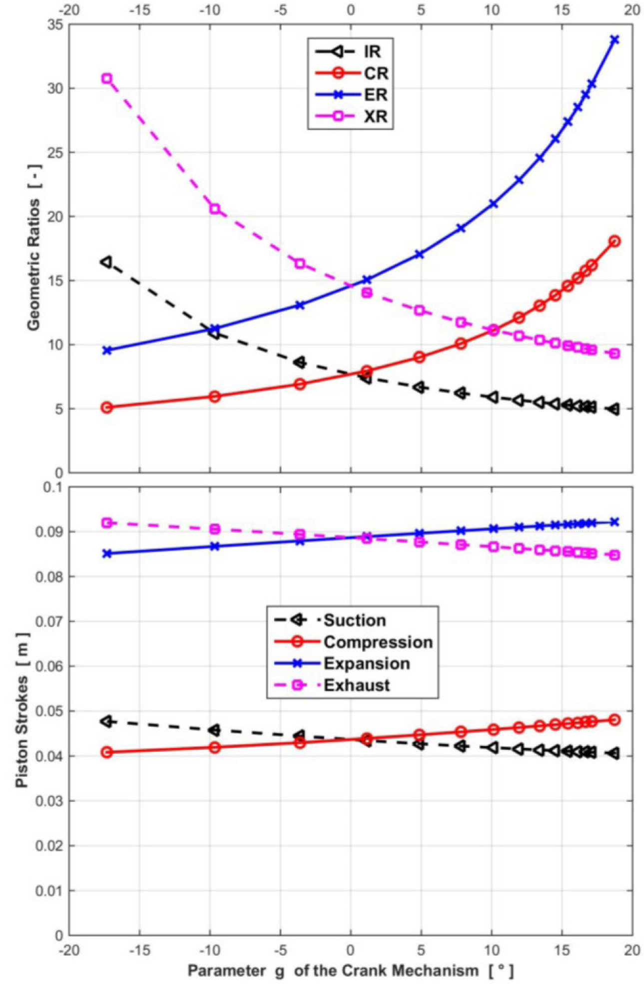

Fig. 22. Geometric Ratios and Piston Strokes for Intake, Compression, Expansion and Exhaust over Parameter "g" for the 2nd Variant of the ACM (see Appendix 2)

The following figures present the simulation results for three values of the CR for both the Seiliger and the Real-Atkinson cycles when using the 2nd variant of the ACM. The maximum pressure values of the cycles are not kept identical (see Fig. 24). The free exhaust ratios ϕ_{ex} were kept identical in all simulations, i.e. we can assure similar conditions for the cylinder exhaust and, thus, for the levels of the cylinder back pressure and temperature (i.e. equivalent to p_{MP12} and T_{MP12} from the BOOST model, see Fig. 7). The aspirated gas mass of the Seiliger cycle is nearly two times bigger than in the Atkinson cycles (see Fig. 25). As expected, the IFCE (see Fig. 26) of the Seiliger cycle is lower than that of the Atkinson cycles because of the truncated expansion of the Seiliger cycle and of the truncated compression of the Atkinson cycle.

In the case of the Atkinson cycle with CR = 5.1, the corresponding CR based on the total displacement (i.e., as in Seiliger cycle) is $CR_{AtoS} = 9.56$. That enables the IFCE comparison of this Atkinson cycle (with CR = 5.1) with that of the Seiliger cycle with CR = 11.1 (see Fig. 26 and 27), even though the aspirated mass (see Fig. 25), and as a result the maximal pressure (see Fig. 24) and IMEP (see Fig. 27), are quite different. Although the converted CR_{AtoS} of the Atkinson cycle is much smaller than that of the Seiliger cycle, the IFCE reaches in the both cycles the same level. This is possible as a result of the shortened compression and the increase of the boost pressure in the Atkinson cycle.

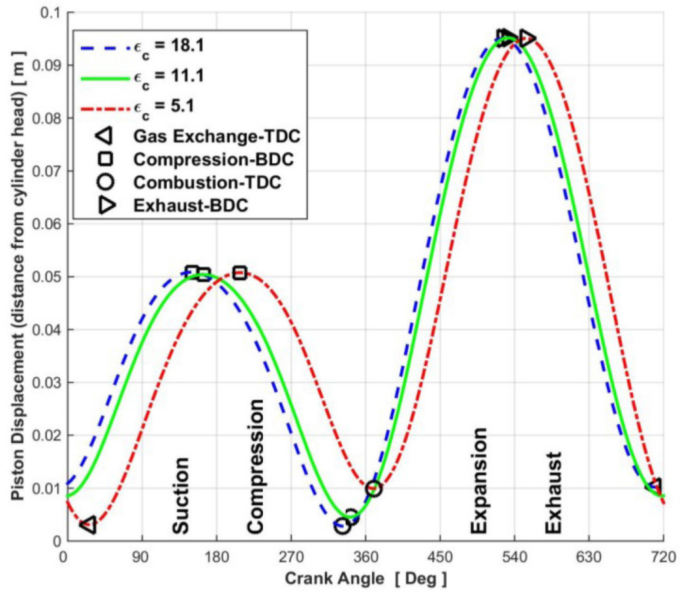

Fig. 23. Piston Displacement, CA - Diagram for three CR (i.e. ε_C) Values at 2nd Variant of the ASC. The CA values are doubled here for convenience.

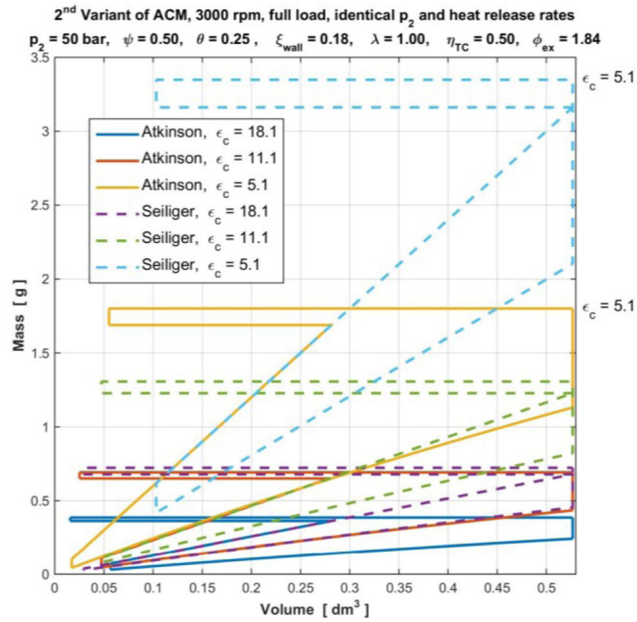

Fig. 25. Gas Mass, Volume - Diagram regarding the CR Variation (ε_C)

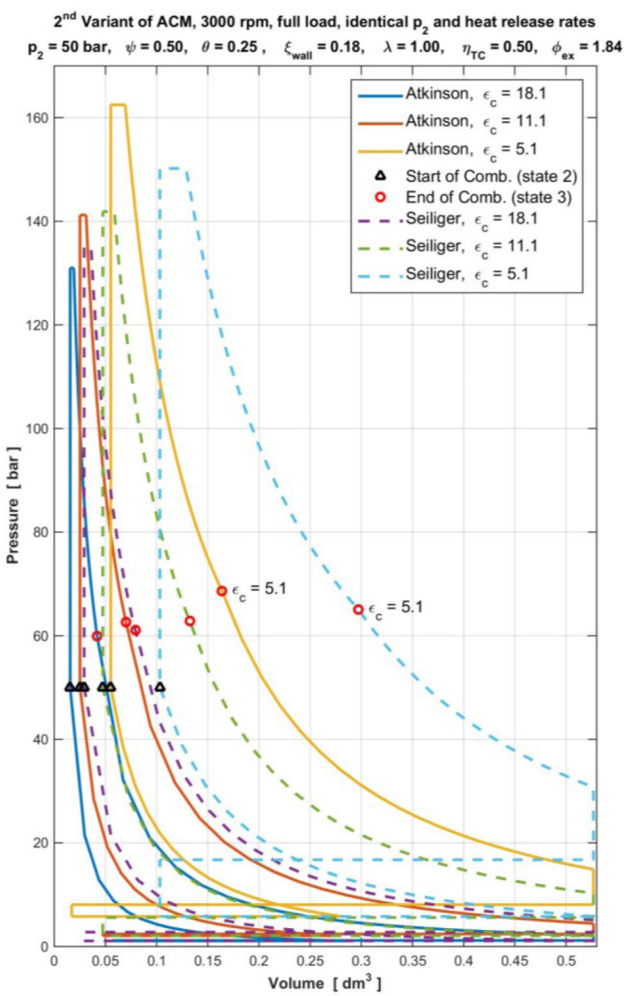

Fig. 24. Pressure, Volume - Diagram regarding the CR Variation (ε_C)

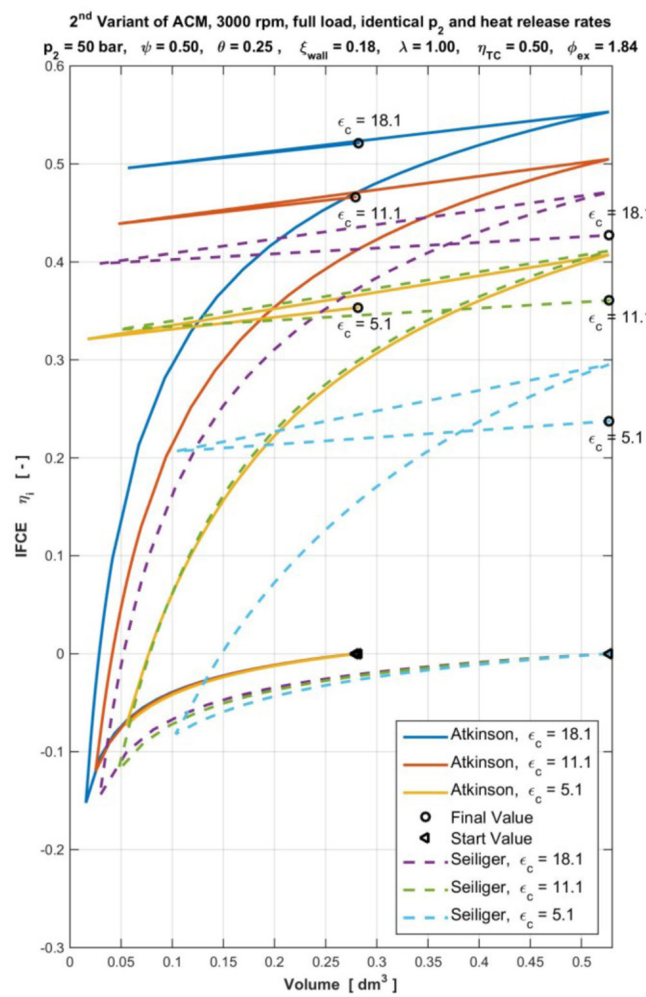

Fig. 26. IFCE, Volume - Diagram regarding the CR Variation

The performances of both cycles over the full variation range of CR values are shown in Fig. 27. The boost pressure (p_C) and temperature are kept identical in both cycles (see below the diagram of Fig 27). The cylinder back pressure (p_T) values are different because of the different gas mass that is exhausted in both cycles (see Fig. 25).

The IFCE improvement of the Real-Atkinson cycle when compared to the Seiliger cycle (i.e. $\Delta(\eta i)/\eta_{iS}$, see top diagram of Fig. 27) reaches more than 20% at all operating points and it increases by higher IMEP values.

Strategy for Load Control

The exhaust residual gas per cycle (internal EGR, see top diagram of Fig. 27) is decreased in the Atkinson cycle by increasing of the IMEP. In this case, the available cylinder volume for the intake of fresh charge is bigger. On the other hand, the intake stroke increases with the reduction of the CR (see Fig. 22 and Fig. 23). In conclusion both of these facts compensate partially by full load the shortened intake stroke of the Atkinson cycle. Accordingly, the IMEP reduction seen in the Atkinson cycle compared to the Seiliger cycle is not very significant (see the middle diagram of Fig. 27).

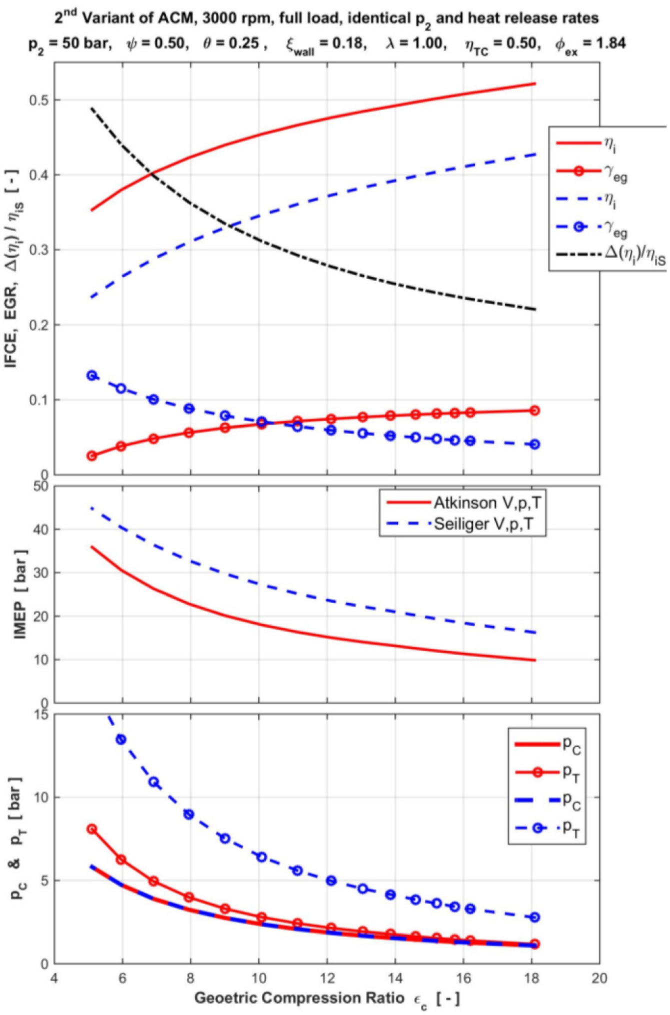

Fig. 27. Performances of the Atkinson and Seiliger Cycles regarding the CR Variation

By using such an asymmetrical crank mechanism with a variable CR, it is possible to achieve the Real-Atkinson cycles of turbocharged engines for part and full loads even without the AFR variation (e.g. with stoichiometric), the throttling or the excessive external EGR. If the asymmetrical crank mechanism also enable the CR variation for each cylinder separately, it is possible to deactivate selectively one or more cylinders by reducing the CR and shutting off of the fueling.

Summary/Conclusions

The implementation of the Real-Atkinson cycles for turbocharged engines using asymmetrical crank mechanisms offers the following advantages: a) relatively high IMEP, b) higher IFCE, leading to fewer CO_2 emissions and c) lower temperatures during the combustion stage, leading to fewer NO_x emissions.

In order to achieve this, the engine requires (in addition to variable valves timing etc.) the use of turbocharger systems with at least two stages, which must be adapted accordingly and controlled with the help of bypasses to maximize their performance. As a result, their optimization is very time consuming.

The comparisons between the V,p,T-model and BOOST simulations shown in this paper indicate that this ideal V,p,T-model can simulate a real model (in this case BOOST) relatively accurately and can predict correctly the upper limit of the cycle performances under the given engine operating conditions.

References

1. Muta, K., Yamazaki, M., and Tokieda, J., “Development of New-Generation Hybrid System THS II - Drastic Improvement of Power Performance and Fuel Economy,” SAE Technical Paper 2004-01-0064, 2004, doi:10.4271/2004-01-0064.
2. Weinowski, R., Sehr A., Wedowski, S., Heuer, S., Hamm, T., Tiemann, C., “Future downsizing of S.I. engines - potentials and limits of 2- and 3-cylinder concepts”, Vienna Motor Symposium, 2009.
3. Korte, V., Lumsden, G., Fraser, N., Hall, J., “30% higher efficiency at 50% less displacement”, MTZ 2010.
4. Schutting, E., Neureiter, A., Fuchs, Ch., Schwarzenberger, T. et al, “Miller- and Atkinson-Cycle for Supercharged Diesel Engines”, MTZ 06, 2007 (German).
5. Gheorghiu, V.: “CO_2-Emission Reduction by Means of Enhancing the Thermal Conversion Efficiency of ICE Cycles”, SAE International Powertrains, Fuels & Lubricants Congress, 2010, Rio de Janeiro, Brazil.
6. Heywood, J. B., “Internal Combustion Engine Fundamentals”, MacGraw-Hill Book Company, 1988.
7. Pischinger, A., Kraβnig, G., Taucar, G., & Sams, Th., “Thermodynamic of Internal Combustion Engines” (German), Springer-Verlag, Wien New York, 1989.
8. Adachi, S., Hagihara, H., “The renewed 4-Cylinder Engine Series for Toyota Hybrid System”, Vienna Motor Symposium, 2012.
9. Patent US 367496 (A), 1887.

10. Patent Application DE 10 2013 003682 (A1).
11. Patent Application EP 2772624 (A1), 2014.
12. Patent US 1326129 A, 1919.
13. Patton, K., Nitschke, R., and Heywood, J., "Development and Evaluation of a Friction Model for Spark-Ignition Engines," SAE Technical Paper 890836, 1989, doi:10.4271/890836.

Acknowledgments

My special thanks to Mr. Dave Roth for his review and very valuable comments.

Abbreviations

ACM - Asymmetrical Crank Mechanism

AFR - Air-Fuel Ratio

BMEP - Break Mean Pressure

CA - Crank Angle

CR - geometric Compression Ratio

EGR - Exhaust Gas Recirculation

EOP - Engine Operating Point

ER - geometric Expansion Ratio

ICE - Internal Combustion Engine

IFCE - Indicated Fuel Conversion Efficiency

IMEP - Indicated Mean Pressure

IVOT - Intake Valve Opening Time

IR - geometric Intake Ratio

LIVC - Late Intake Valve Closed

MPx - Measuring Point x in BOOST model

SCM - Symmetrical Crank Mechanism

SOC - Start of Combustion

TC - Turbocharger

Tx - Turbine x (here x = 1 to 3)

V,p,T - Model of an ideal cycle where the heat is partially released isochorically, isobarically and isothermally

UD - Ultra-Downsizing

XR - geometric Exhaust Ratio

eo - Exhaust Valve Opening

ec - Exhaust Valve Closing

io - Intake Valve Opening

ic - Intake Valve Closing

$\boldsymbol{\mu_{Tx}}$ - Discharge Coefficient of the Turbine x

APPENDIX

Appendix 1

Symbol	Meaning	Units
$\varepsilon_c = \frac{V_1}{V_2} = \frac{V_{in}}{V_c}$	volumetric compression ratio	-
$\varepsilon_e = \frac{V_5}{V_2} = \frac{V_e}{V_c}$	volumetric expansion ratio	-
$\varepsilon_i = \frac{V_1}{V_7} = \frac{V_{in}}{V_{out}}$	volumetric intake ratio	-
$\varepsilon_x = \frac{V_5}{V_6} = \frac{V_e}{V_{out}}$	volumetric exhaust ratio	-
$V_c = V_2 = V_{3v}$	cylinder volume at end of compression	m^3
$V_e = V_4 = V_5 = V_{max}$	cylinder volume at end of expansion	m^3
$V_{out} = V_6 = V_7$	cylinder volume at end of emptying	m^3
$V_{disp} = V_{max} \cdot \left(1 - \min\left(\frac{1}{\varepsilon_e}, \frac{1}{\varepsilon_x}\right)\right)$	cylinder displacement	m^3
$p_{max} = p_{3v} = p_{3p}$	maximal pressure on cycle	Pa
$T_{max} = T_{3p} = T_3$	maximal temperature on cycle	K
$p_1 = p_C$	cylinder pressure in state 1	Pa
$T_1 = T_C$	cylinder temperature in state 1	K
$m_1 = \frac{p_1 \cdot V_1}{m_1 \cdot T_1}$	cylinder gas mass in state 1	kg
$V_1 = V_{max} \cdot \frac{\varepsilon_c}{\varepsilon_e}$	cylinder volume in state 1	m^3
$m_a = m_1 \cdot \frac{\varepsilon_x - 1}{\varepsilon_x}$	aspirated charge mass per cycle	kg
$m_{max} = m_1 + m_f$	maximal gas mas on cycle	kg
$m_f = \frac{m_1 \cdot (1 - \gamma)}{\lambda \cdot L_{st}}$	fuel mass per cycle	kg
γ	exhaust rest gase rate per cycle	-
λ	air-exces ratio (AFR)	-
L_{st}	stoichiometric air requirement ratio	$\frac{kg}{kg}$
κ_c, κ_e	isentropic exponents and	-
$c^\circ_{p.c}, c^\circ_{v.c}$ $c^\circ_{p.e}, c^\circ_{v.e}$	isobaric (p) & isochoric (v) specific heat capacities on compression (c) resp. expansion (e)	$\frac{J}{kg \cdot K}$
R	ideal gas constant	$\frac{J}{kg \cdot K}$
H_u, H_{vap}	fuel lower heating & vaporisation heat values	$\frac{J}{kg}$
$Q_{rel} = m_f \cdot H_u$	cylinder released heat	J
η_b	released fuel energy completeness	-

Symbol	Meaning	Units
Q_{wall}	heat transfer to cylinder wall	J
$Q_{disp} = Q_{rel} \cdot \eta_b + Q_{wall}$	disposable heat on cycle	J
p_C	charge pressure after cooler	Pa
T_C	charge temperature after cooler	K
p_T	pressure before turbine	Pa
T_T	temperature before turbine	K
p_u	ambient pressure	Pa
$\delta = \dfrac{Q_{disp}}{m_{max} \cdot c^{\circ}_{v.c} \cdot T_1}$	relative released heat as measure of engine load	-
$Q_{disp.v}$	isochoric part of Q_{disp}	J
$\psi = \dfrac{Q_{disp.v}}{Q_{disp}}$	isochoric released heat fraction	-
$Q_{disp.t}$	isothermal part of Q_{disp}	J
$\theta = \dfrac{Q_{disp.t}}{Q_{disp}}$	isothermal released heat fraction	-
$1 - \psi - \theta = \dfrac{Q_{disp.p}}{Q_{disp}}$	isobaric released heat fraction	-
$\phi_{ex} = \dfrac{p_4}{p_5}$	pressure ratio for free exhaust	-
$Q_{disp.p}$	isobaric part of Q_{disp}	J
$\eta_i = \dfrac{-W_{cycle}}{Q_{rel}}$	indicated fuel conversion efficiency IFCE	-
W_{cycle}	work on the all cycle	J
$p_i = \dfrac{-W_{cycle}}{V_{disp}}$	indicated mean pressure IMEP	Pa
$\eta_{sC}, \eta_{sT}, \eta_{TC}$	isentropic efficiency of compressor, turbine and turbocharger	-
W_{TTu}	turbine work between p_T and p_u	J
W_{CuC}	compressor work between p_u and p_C	J

$$m_2 = m_1 \qquad p_2 = p_1 \cdot \varepsilon_c^{\kappa_c} \qquad V_2 = \frac{V_1}{\varepsilon_c} \qquad T_2 = T_1 \cdot \varepsilon_c^{\kappa_c - 1}$$

$$m_{3v} = m_{max} = m_1 \cdot \left(1 + \frac{1-\gamma}{\lambda \cdot L_{st}} \cdot \frac{\varepsilon_x - 1}{\varepsilon_x}\right)$$

$$p_{3v} = p_{max} \qquad V_{3v} = V_2 \qquad T_{3v} = \frac{m_1}{m_{max}} \cdot \frac{p_{max}}{p_C} \cdot \frac{T_1}{\varepsilon_c}$$

$$\theta = 1 - \psi - \frac{\kappa_e \cdot (\kappa_c - 1)}{(\kappa_e - 1) \cdot \delta} \cdot \left(\frac{T_{max}}{T_1} - \frac{m_1}{m_{max}} \cdot \frac{p_{max}}{p_C} \cdot \frac{1}{\varepsilon_c}\right)$$

$$m_{3p} = m_{max} \qquad V_{3p} = V_{3v} \cdot \frac{T_{max}}{T_{3v}} \qquad T_{3p} = T_3 = T_{max}$$

$$m_3 = m_{max} \qquad V_3 = \frac{m_{max} \cdot R \cdot T_{max}}{p_{max}} \cdot \exp\left[\frac{\theta \cdot \delta \cdot T_1}{(\kappa_c - 1) \cdot T_{max}}\right]$$

$$m_4 = m_{max}$$

$$V_4 = V_{max} \qquad p_4 = p_3 \cdot \left(\frac{V_3}{V_4}\right)^{\kappa_e} \qquad T_4 = T_3 \cdot \left(\frac{V_3}{V_4}\right)^{\kappa_e - 1}$$

$$p_5 = \frac{p_4}{\phi_{ex}} \qquad \text{where e.g.} \qquad \phi_{ex} = \left(\frac{2}{1+\kappa_e}\right)^{\frac{\kappa_e}{\kappa_e - 1}}$$

$$W_{CuC} = c^\circ_{p.c} \cdot \frac{m_a \cdot T_u}{\eta_{sC}} \cdot \left[\left(\frac{p_C}{p_u}\right)^{\frac{\kappa_c - 1}{\kappa_c}} - 1\right]$$

$$W_{TTu} = \eta_{sT} \cdot (m_a + m_f) \cdot c^\circ_{p.e} \cdot T_T \cdot \left[1 - \left(\frac{p_u}{p_T}\right)^{\frac{\kappa_e - 1}{\kappa_e}}\right]$$

$$W_{CuC} = W_{TTu} \qquad k_1 = \eta_{TC} \cdot \frac{1 - \gamma + \lambda \cdot L_{st}}{\lambda \cdot L_{st}} \cdot \frac{\kappa_e}{\kappa_e - 1} \cdot \frac{\kappa_c - 1}{\kappa_c} \cdot \frac{1}{T_u}$$

$$p_C = p_u \cdot \left[1 + k_1 \cdot T_4 \cdot \left[\left(\frac{p_5}{p_4}\right)^{\frac{\kappa_e - 1}{\kappa_e}} - \left(\frac{p_u}{p_4}\right)^{\frac{\kappa_e - 1}{\kappa_e}}\right]\right]^{\frac{\kappa_c}{\kappa_c - 1}}$$

$$T_5 = T_4 \cdot \left(\frac{p_5}{p_4}\right)^{\frac{\kappa_e - 1}{\kappa_e}} \qquad V_5 = V_{max} \qquad p_5 = p_T \qquad T_T = T_5 \qquad m_5 = \frac{p_5 \cdot V_5}{R \cdot T_5}$$

$$p_6 = p_5 \qquad V_6 = \frac{V_{max}}{\varepsilon_x} \qquad T_6 = \left(2 \cdot T_5 - T_4\right) \cdot k_{T6}$$

$$m_6 = \frac{p_6 \cdot V_6}{R \cdot T_6}$$

$$\begin{aligned} W_{cycle} = {} & \frac{p_C \cdot V_{max}}{\kappa_c - 1} \cdot \frac{\varepsilon_c}{\varepsilon_e} \cdot \left(\varepsilon_c^{\kappa_c - 1} - 1\right) + \frac{p_{max} \cdot V_{max}}{\varepsilon_e} \dots \\ & + \left(-m_{max}\right) \cdot R \cdot T_{max} - \theta \cdot \delta \cdot \frac{m_{max} \cdot R \cdot T_1}{\kappa_c - 1} \dots \\ & + \frac{m_{max} \cdot R \cdot T_{max}}{\kappa_e - 1} \cdot \left[\left(\frac{V_3}{V_{max}}\right)^{\kappa_e - 1} - 1\right] \dots \\ & + p_T \cdot V_{max} \cdot \frac{\varepsilon_x - 1}{\varepsilon_x} - p_C \cdot V_{max} \cdot \left(\frac{\varepsilon_c}{\varepsilon_e} - \frac{1}{\varepsilon_x}\right) \end{aligned}$$

$$k_{T6} = \frac{\text{area}(T, s) \cdot m_{max}}{W_{cycle}} \qquad \gamma = \frac{m_6}{m_1} \qquad \text{iterative}$$

Appendix 2

Asymmetrical Crank Mechanism (ACM) can be designed in many variants. E.g. in [10] and [11] are presented five such variants. This appendix features only a brief presentation of the 1st and 2nd variants (see Fig. A2-1 and A2-2).

The 1st variant of ACM uses the 3:2 ratio and the 2nd variant the 3:1 ratio between the teeth number of the ring (11) and the planet gears (10). Therewith the four strokes are generated in the 1st variant in two revolutions and in the 2nd variant in only one revolution of the crankshaft.

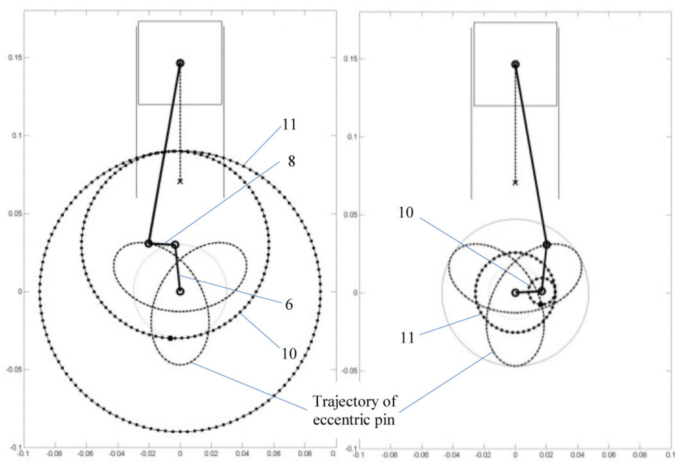

Fig. A2-1. Schematic design of the 1st (left) and 2nd variants of the ACM for equal piston strokes lengths. The eccentric radius (8) (or "exx") is the distance between the crank pin (7) and the eccentric pin (9) (see Fig. A2-2).

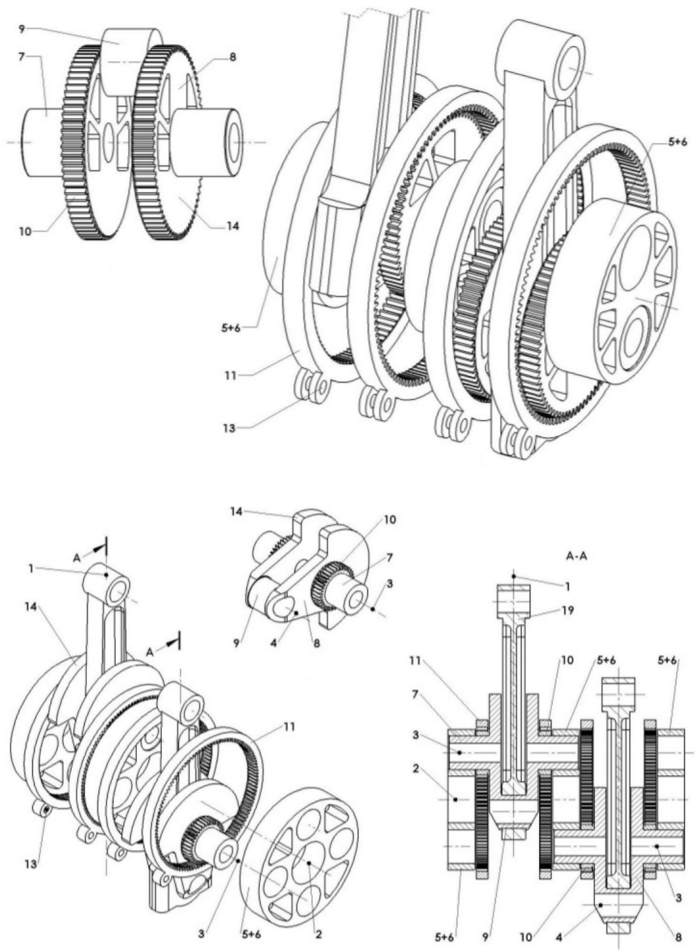

Fig. A2-2. Exemplary CAD Designs of the 1st (top) and the 2nd Variants for 2 cylinder ACM. The shaft journal (5) and the crank (6) form together the component (5+6). The distance between crank pin (7) and the eccentric pin (9) defines the eccentric radius. The planet gears (10), the eccentric web (8) and pin (9) and the counterweight (14) form together the eccentric crank. The ring gears (11) are guided in the crankcase and can be angularly twisted with respect to the center position by applying a force to eyelet (13) [10], [11].

Appendix 3

The following investigation cases (by means of BOOST® simulations) are performed for a small turbocharged DI SI 3 cylinder engine with classical (symmetric) crank mechanism. The sole purpose of this appendix is to investigate in detail the influence of the Intake Valve Opening Time (IVOT) - when the intake valve opening (io) is unchanged and only its closing (ic) is varied - on the indicated and the effective efficiencies. In order for these results to be transferable to naturally aspirated engines, the boost pressure (p_C) is kept constant (naturally aspirated engines have the “boost pressure” almost equal to the ambient pressure and thus constant). All parameters of this model, with the exception of the intake valve closing and thus of IVOT, are kept unchanged during these simulations (i.e. the SOC is not adapted here for knock limitation and/or optimizing of the MFB50 position).

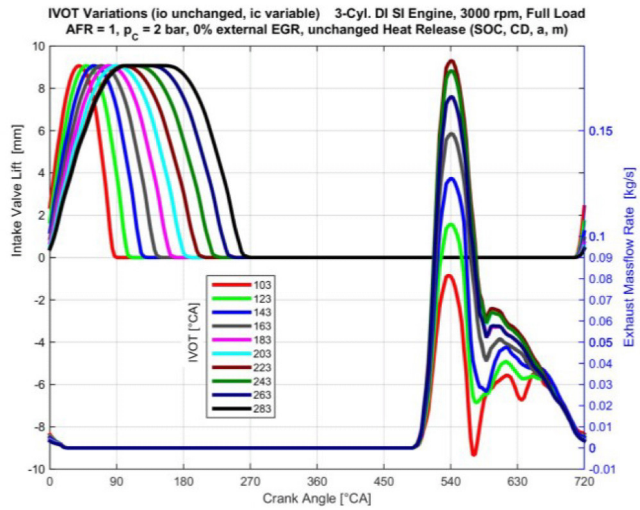

Fig. A3-1. Intake Valve Lift, CA Diagram (left axis) and Exhaust Massflow Rate, CA (right axis) Diagram.

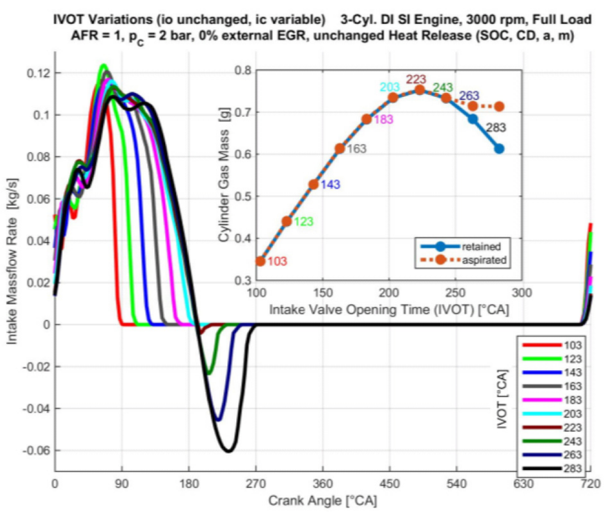

Fig. A3-2. Intake Massflow Rate, CA Diagram (left axis) and Cylinder Gas Mass, IVOT Diagram (inserted).

The intake valve lift and the exhaust massflow rate curves are presented in Fig. A3-1. The IVOT = 103°CA corresponds to a strong Miller cycle and the IVOT = 283°CA to a strong Quasi-Atkinson cycle.

For the IVOT = 103°CA (red curve) the free exhaust occurs very sluggishly because of the low cylinder pressure level to the exhaust valve opening (eo = 490°CA) (see Fig. A3-4 and Fig. A3-6) and the aspirated gas mass, peak cylinder pressure and temperature reach their minima between these cases (see inserted diagram in Fig. A3-2, Fig. A3-3, A3-4, A3-5) and the exhaust residual gas its maximum (see Fig. A3-10).

In the variants up to IVOT = 223°CA, the entire aspirated gas mass is kept inside the cylinder and thus no difference occurs between the aspirated and the retained mass (see inserted diagram in Fig. A3-2, and Fig. A3-3 on the top-right side).

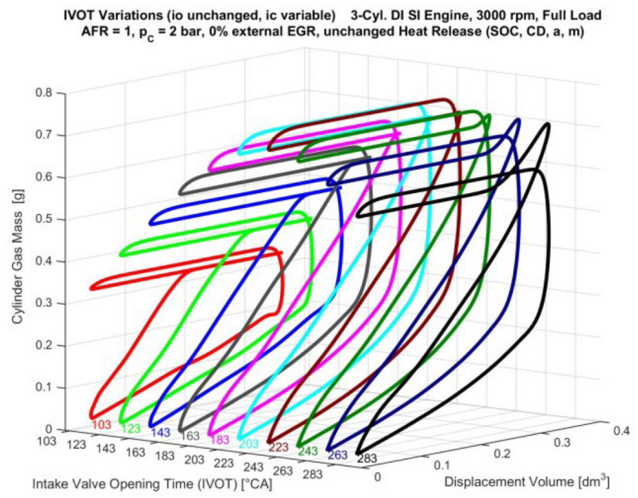

Fig. A3-3. Gas Mass, Volume 3D-Diagram.

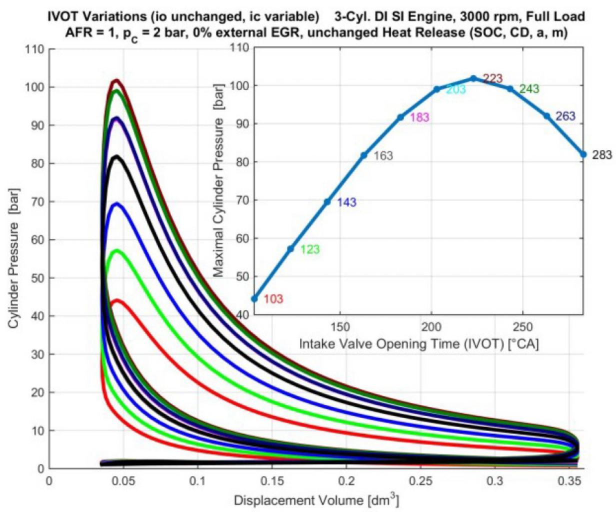

Fig. A3-4. Pressure, Volume Diagram and Maximal Pressure, IVOT Diagram (inserted).

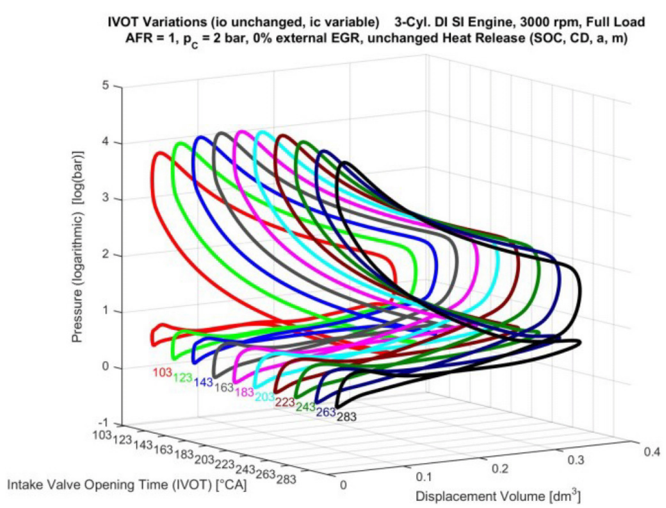

Fig. A3-5. Pressure, Volume, IVOT 3D-Diagram.

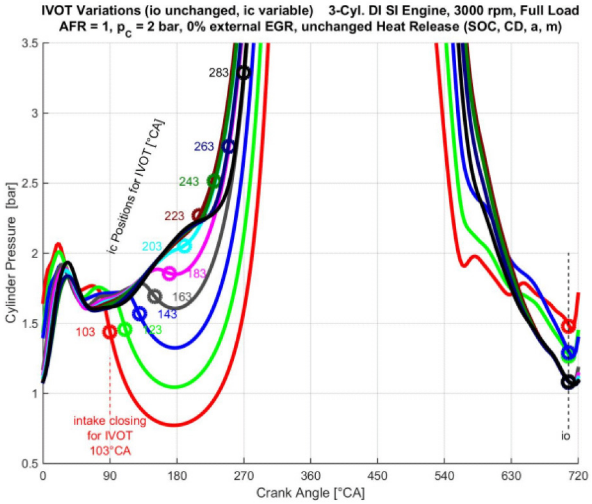

Fig. A3-6. Pressure, CA Diagram with Intake Valve Timing (io, ic) Positions for all IVOT Variants.

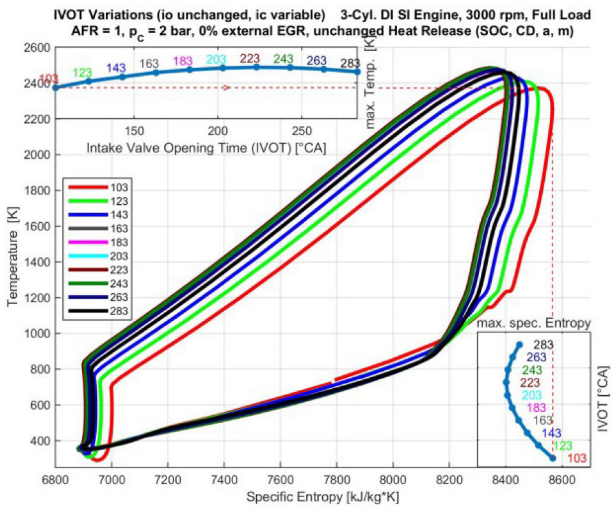

Fig. A3-7. Temperature, Specific Entropy (T,s) Diagram with inserted Diagrams of their Maxima.

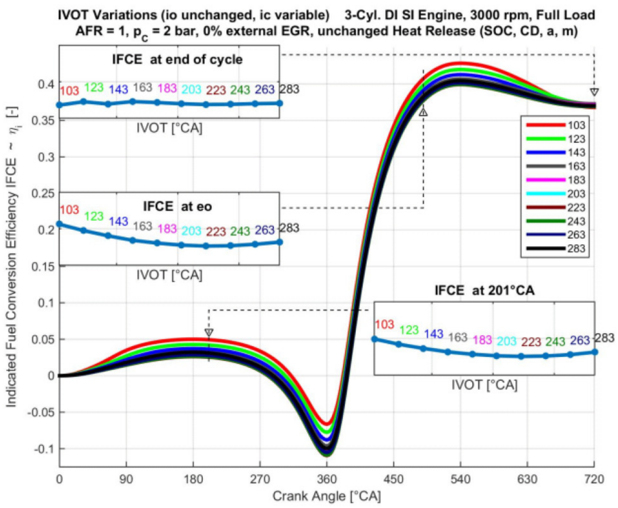

Fig. A3-8. IFCE, CA Diagram and IFCE, IVOT Diagrams in three characteristic Cuts (see Insertions).

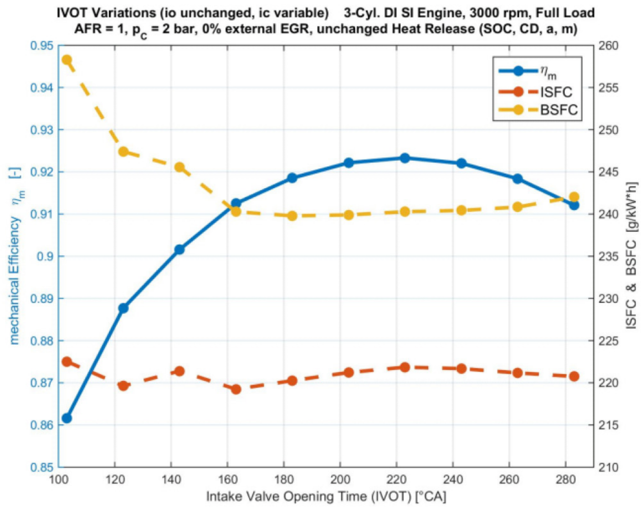

Fig. A3-9. Mechanical Efficiency, IVOT Diagram (left axis) and ISFC & BSFC, IVOT (right axis) Diagrams.

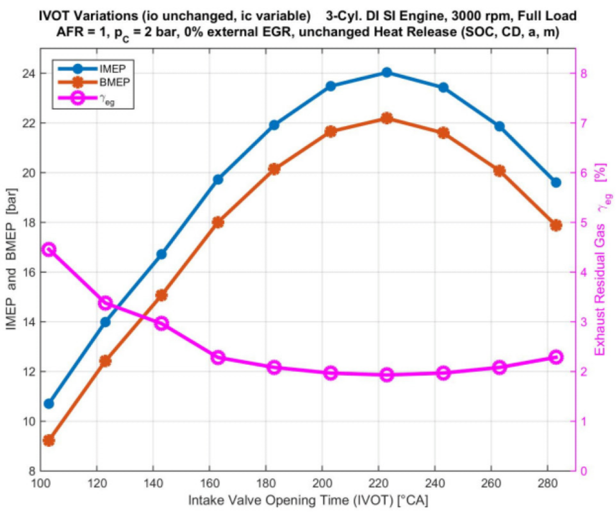

Fig. A3-10. IMEP & BMEP, IVOT Diagrams (left axis) and Exhaust Residual Gas Rate, IVOT (right axis) Diagram.

For the variants with an IVOT greater than 223°CA, Quasi-Atkinson cycle are produced, where a part of the aspirated gas mass flow back to the intake manifold. These are characterized by the negative massflow rate through the intake valve (see Fig. A3-2) and differences between (maximal) aspirated and retained gas mass (see diagram inserted in Fig. A3-2, and Fig. A3-3 on the top-right side).

Although the gas mass retained in the cylinder for IVOT = 103°CA reaches only 46% of that for IVOT = 223°CA (IVOT variant with maximum gas mass), the maximum temperature on the cycle is reduced (which is the aim of Miller cycle) by less than 5% (see Fig. A3-7). The T,s diagram from Fig. A3-7 does not help much in evaluating the indicated efficiency, since the cylinder gas mass changes greatly during the gas exchange processes (open cycle).

In Fig. A3-8 the IFCE evolutions are shown over the crank angle. Although these IFCE curves show differences between IVOT variations in the cuts to the crank angle positions 201°CA and 490°CA (at the exhaust valve opening), the IFCE values at the end of the cycle are approximately the same for all IVOT variants. Therefore, the IVOT variations for the thermodynamic efficiency are neutral.

When the friction model of Patton, Nitschke and Heywood [13] is taken into account, the brake efficiency η_e and thus the BSFC are quite different for the IVOT variants and reach their optimum for the Seiliger cycles (see Fig. A3-9).

In conclusion the application of Miller and Quasi-Atkinson cycles offer no advantages from a strictly thermodynamic point of view. The improved efficiency reported by Toyota, Honda, etc., which make use of LIVC, is based more on the optimization of many parameters, such as ignition timing, MFB50 position etc, and of dethrottling by low loads (i.e. the reduction of the retained gas mass in cylinder, see Fig. A3-2, A3-3 and A3-10), because the dethrottling through the use of Miller or Quasi-Atkinson cycle is more (brake) efficient than the classical throttling for the Seiliger cycle at the throttle valve.

The Engineering Meetings Board has approved this paper for publication. It has successfully completed SAE's peer review process under the supervision of the session organizer. The process requires a minimum of three (3) reviews by industry experts.

ISSN 0148-7191

http://papers.sae.org/2015-01-1252